UNIVERSITÀ DEGLI STUDI DI PARMA

Dottorato di Ricerca in Tecnologie dell'Informazione

XXIII Ciclo

co-tutela di tesi con

TÉLÉCOM BRETAGNE

En habilitation conjointe avec l'Université de Bretagne Sud

École Doctorale - **sicma**

ADVANCED LOW-COMPLEXITY MULTIUSER RECEIVERS

Coordinatore:

Chiar.mo Prof. Carlo Morandi

Tutors:

Chiar.mo Prof. Giulio Colavolpe

Chiar.mo Prof. Alexandre Graell i Amat

Chiar.ma Prof.ssa Catherine Douillard

Dottorando: *Amina Piemontese*

January 2011

Contents

List of acronyms

AM amplitude modulation

APP a posteriori probability

APSK amplitude-phase shift keying

AWGN additive white Gaussian noise

BCJR Bahl, Cocke, Jelinek, Raviv

BER bit error rate

BPSK binary phase shift keying

CDMA code division multiple access

CPM continuous phase modulation

CRB Cramér-Rao lower bound

DA data-aided

DVB-RCS Digital Video Broadcating Return Channel via Satellite

eBCH extended Bose, Ray-Chaudhuri, Hocquenghem

EXIT extrinsic information transfer

FBA forward backward algorithm

FDM frequency division multiplexing

FG factor graph

FPGA field programmable gate array

IBO input back-off

ICI intercarrier interference

i.i.d. independent and identically distributed

IMUX input demultiplexer filter

IR information rate

ISI intersymbol interference

LDPC low-density parity-check

LUT look-up table

MAI multiple-access interference

MAP maximum a posteriori probability

MI mutual information

MMSE minimum mean square error

MSE mean square error

MSK minimum shift keying

MUD multiuser detection

OFDM orthogonal frequency division multiplexing

O-MUD optimal multiuser detercor

OMUX output multiplexer filter

PM phase modulation

pdf probability density function

pmf probability mass function

PN phase noise

PSD power spectral density

PS-SPA parallel-schedule SPA

QAM quadrature amplitude modulation

REC rectangular

RC raised-cosine

SCCPM serially-concatenated continuous phase modulation

SE spectral efficiency

SIC soft interference cancellation

SISO soft-input soft-output

SNR signal-to-noise ratio

SPA sum-product algorithm

SS-SPA serial-schedule SPA

SUD single-user detector

TWTA traveling wave tube amplifier

Foreword

This thesis deals with multiuser detection (MUD) for spectrally-efficient wireless communication systems. The aim of this work is to propose new advanced low-complexity multiuser receivers with near-optimal detection performance. We consider frequency division multiplexing (FDM) satellite systems where each user employs a continuous phase modulation (CPM), serially concatenated with an outer code through an interleaver, and iterative detection/decoding. We also consider linear channels impaired by additive white Gaussian noise (AWGN), focusing on FDM systems where adjacent channels are allowed to overlap in frequency, and on code division multiple access systems (CDMA).

For the considered scenarios, we propose detection schemes with an excellent performance/complexity tradeoff which allow us to implement transmission schemes with unprecedented spectral efficiency (SE) at a price of a limited complexity increase with respect to a classical single-user receiver which neglects the interference.

Overview of the Thesis

This thesis is organized as follows.

Chapter 1 introduces the thesis and describes some mathematical and graphical frameworks used in this work. In particular, we briefly introduce the framework based on factor graphs (FGs) and the sum-product algorithm (SPA) and we explain how to compute the ultimate performance limits of channels

with memory.

In Chapter 2, we focus on FDM systems where each user employs a CPM. We compare, from an information-theoretic point of view, the performance of a satellite transmission scheme employing CPMs with that of a scheme employing linear modulations and we show that CPMs are superior in terms of SE. We discuss the application of suboptimal reduced-complexity MUD schemes to the FDM-CPM scenario and propose a new algorithm, which is obtained by using the FG/SPA tool. Possible extensions of this new scheme are also discussed. We evaluate the ultimate performance limits imposed by FDM-CPM systems when multiuser detectors are employed at the receiver side. We consider practical serially-concatenated continuous phase modulation schemes employing suboptimal multiuser detectors as inner soft-input soft-output (SISO) detector and show that the theoretical limits predicted by the information-theoretic analysis can be approached. Finally, we consider multiuser processing issues, and propose reduced-complexity schemes for MUD in the presence of time-varying phase noise, and data-aided multiuser phase and frequency synchronization schemes.

In Chapter 3, we consider detection over linear channels impaired by AWGN. We present a novel FG describing the system and derive two SISO-detection algorithms. We provide some examples of channels that can be led to the considered model, discussing for each of them the complexity of the optimal maximum a posteriori symbol detector. We report some performance/complexity comparisons between our algorithms and some reference benchmarks, in the case of channels affected by intersymbol interference, CDMA systems and spectrally-efficient FDM systems, which are particular scenarios of the considered general model.

Finally Chapter 4 concludes the thesis giving some remarks on the main results.

Notation

Throughout the thesis, $P(\cdot)$ denotes the probability mass function of a discrete random vector and $p(\cdot)$ denotes the probability density function of continuous random vector.

Sequences are written in lower-case bold fonts and matrices are written in upper-case. Given a generic sequence $\mathbf{x}$, we denote by x_n the n-th element of $\mathbf{x}$ and by $\mathbf{x}_n^k$ the subvector collecting all the elements from index n to index k, with $n < k$. Given a generic matrix $\mathbf{X}$, we denote by $X_{m,n}$ its entry at row m and column n. The symbols $(\cdot)^\dagger$, $(\cdot)^{\mathrm{H}}$, $||\cdot||$, and $E[\cdot]$ denote the transpose operator, the conjugate transpose operator, the 2-norm operator, and the statistical expectation operator, respectively.

The proportionality symbol $\propto$ is used when two quantities differ by factors irrelevant for the detection process.

Chapter 1

Introduction

1.1 Background and Objectives

We consider the design of multiuser detection (MUD) algorithms for wireless communication systems, using the spectral efficiency (SE) as the fundamental figure of merit. Since the spectrum available for wireless data services and systems is a scarse resource, high degree of SE is a common requirement of communication systems. A way of increasing the SE is to adopt a nonorthogonal multiplexing strategy and to intentionally introduce multiple-access interference (MAI). For example, the SE of frequency division multiplexing (FDM) systems can be increased by reducing the spacing between two adjacent channels, thus allowing overlap in frequency and hence admitting a certain amount of interference [1, 2].[1] But the MAI becomes the major impediment to the overall system performance and MUD techniques are mandatory. MUD refers to the process of demodulating signals in the presence of multiaccess interference [3] and can provide very substantial performance gains over conventional single-user detection techniques for spectrally-efficient communication systems.

[1] In this context, the terms "single-channel" and "multi-channel" would be more suited than "single-user" and "multiuser". However, in this thesis we will use the terms "users" and "channels" interchangeably.

This performance comes at the expense of a complexity increase. In fact, the complexity of the optimal multiuser detector (O-MUD) increases exponentially with the number of interferers, and suboptimal detection schemes are required. Therefore, the design of low-complexity suboptimal multiuser detectors able to effectively cope with the increased interference is a key element to make MUD appealing for real-world applications. In this thesis, we address this issue and we resort to the powerful framework based on factor graphs (FGs) and the sum-product algorithm (SPA) [4] to design novel detection algorithms. The FG/SPA tool has been often used in the past to reinterpret known algorithms, but it is also very useful for deriving new detection schemes with an unprecedented complexity/performance trade-off [5–9] or for applications where traditional probabilistic methods fail [10].

In this thesis, we consider FDM systems where each user employs a continous phase modulation (CPM). CPM is appealing in satellite communications for its robustness to non-linearities, its claimed power and SE, and its recursive nature which allows to employ it in serially concatenated schemes [11–13]. The literature on MUD for FDM-CPM systems is very poor and essentially focuses on binary schemes, such as Gaussian minimum shift keying. In [14], the theoretical limits of a multiuser communication system using serially-concatenated CPMs (SCCPMs) over an additive white Gaussian noise (AWGN) channel were investigated. However, reduced-complexity MUD techniques were not considered in [14]. Suboptimal low-complexity MUD techniques based on soft interference cancellation (SIC) (e.g., see [15, 16]) from the code division multiple access systems (CDMA) literature have been derived relying on a Gaussian approximation of the MAI. We extend these suboptimal MUD schemes to the FDM-CPM scenario. We also propose a new scheme which is obtained by means of some graphical manipulations on the FG representing the joint a posteriori probability mass function (pmf) of the transmitted symbols, rather than assuming the interference as Gaussian, as suggested in [15–17]. This new algorithm outperforms all other suboptimal MUD algorithms in both performance and complexity.

With the aim to design highly efficient communication systems, we evaluate the asymptotic performance of FDM-CPM systems when multiuser detectors are employed and compute the achievable information rate (IR) and the SE. We use the information-theoretic approach to optimize the channel spacing among adjacent channels so that the achievable SE is maximized. Using the optimized parameters, we then consider practical schemes where CPMs are serially concatenated with an outer code through an interleaver, and the proposed suboptimal multiuser detector is employed as inner soft-input soft-output (SISO) detector. We analyze the convergence behavior of joint multiuser detection/decoding by means of an extrinsic information transfer (EXIT) chart analysis and show that the theoretical limits predicted by the information-theoretic analysis can be approached by SCCPM schemes.

In more realistic FDM scenarios, a denser packing has an impact not only on the detection algorithm. In fact, once satisfactorily suboptimal MUD algorithms are available, other subsystems become critical. In particular, carrier synchronization schemes able to cope with the increased interference must be adopted. Hence, we finally consider multiuser processing issues and propose reduced-complexity schemes for MUD in the presence of time-varying phase noise (PN), and multiuser data-aided (DA) phase and frequency synchronization schemes. We show that, by taking into account the increased interference using properly designed multiuser detection and synchronization algorithms, it is possible to implement transmission schemes with unprecedented SE with a computational complexity which increases only linearly with the number of the interfering users.

In this thesis, we also consider detection over linear channels impaired by AWGN. Also in this case, we are interested in spectrally-efficient transmissions, where interference among symbols is intentionally introduced in order to increase the bandwidth efficiency. We start from a very general model, which describes a large variety of scenarios, and introduce a novel FG describing the system, based on which we derive algorithms for SISO detection by means of the SPA. The considered FG is exact, since no approximation is required for

its derivation, but contains cycles, and thus leads to algorithms for approximate maximum a posteriori (MAP) symbol detection [4]. Interestingly, our algorithms are characterized by a complexity that grows only linearly with the number of interferers and, being SISO in nature, can be adopted in turbo processing without additional modifications. To prove their effectiveness, we report simulation results and performance comparisons for some selected scenarios such as CDMA systems employing iterative detection/decoding, and FDM systems with intercarrier interference (ICI) [1,18]. When compared with the existing interference-cancellation algorithms, the proposed schemes result very appealing in terms of tradeoff between performance and computational complexity. In particular, the proposed schemes can approach or even outperform the performance provided by much more complex algorithms.

1.2 General Frameworks

We here describe some frameworks widely used in the remainder of this work. In particular, we briefly introduce the FG/SPA tool, using as reference the excellent tutorial paper [4]. Moreover we summarize the simulation-based method proposed in [19–21] for computing the IR for channels with memory. In Chapter 2 we use this method to evaluate the ultimate performance limits of transmission schemes employing CPMs.

1.2.1 Factor graphs and the sum product algorithm

Let $x_1, x_2, \ldots, x_n$ be a collection of variables, where x_i takes on values on some (usually finite) domain A_i, and let $g(x_1, x_2, \ldots, x_n)$ be a real-valued function of these variables. Suppose that we want to compute the marginal functions associated to $g(x_1, x_2, \ldots, x_n)$, namely the n functions $g_i(x_i)$ defined as

$$g_i(x_i) \triangleq \sum_{\sim\{x_i\}} g(x_1, x_2, \ldots, x_n)\,,$$

where we indicate by $\sum_{\sim\{x_i\}}$ the not-sum or *summary* operator [4], i.e., a sum over all variables exept x_i.

The marginalization of a function is a problem common to many applications. Typically, detection problems need the marginalization of a possibly cumbersome function, depending on many variables. If the function to marginalize can be expressed as the product of simpler functions, each of them depending on a subset of the variables, the marginalization turns out to be less complex. The FGs provide a natural graphical description of the factorization of a "global" function into a product of "local" functions. The SPA works on the FG and computes—either exactly or approximately—the marginal functions derived from the global function.

Suppose that $g(x_1, x_2, \ldots, x_n)$ factors into a product of several local functions f_j, each having a subset $\mathbf{x}_j$ of $\{x_1, x_2, \ldots, x_n\}$ as argument, i.e.

$$g(x_1, x_2, \ldots, x_n) = \prod_{j \in J} f_j(\mathbf{x}_j)\,, \tag{1.1}$$

where J is a discrete index set. The FG of the function g is a bipartite graph which has a variable node for each variable x_i, a factor node for each function f_j, and an edge connecting variable node x_i to function node f_j if and only if x_i is an argument of f_j. The SPA is a message-passing algorithm working over a FG. It consists of the evaluation of "messages" at the nodes of the bipartite graph and the exchange of such messages along the edges. It can be proved that if the FG is acyclic (and hence it admits a tree representation for each variable node) the SPA carries out the exact marginalization of the function represented by the FG. Denoting by $\mu_{x\to f}(x)$ a message sent from variable node x to the factor node f, and by $\mu_{f\to x}(x)$ a message in the opposite direction, the message computations performed at variable and factor nodes are, respectively

$$\begin{aligned}
\mu_{x\to f}(x) &= \prod_{h\in\, n(x)\setminus\{f\}} \mu_{h\to x}(x) \\
\mu_{f\to x}(x) &= \sum_{\sim\{x\}} \left[f(X) \prod_{y\in n(f)\setminus\{x\}} \mu_{y\to f}(y) \right],
\end{aligned}$$

where $n(x)$ is the set of functions f having x as argument, and $X = n(f)$ is the set of arguments of the function f. If the graph is cycle-free, it has a tree representation and the SPA begins by evaluating messages at the leaf nodes, which send to their neighbor nodes an identity message given by $\mu_{x\to f}(x) = 1$ if the leaf is a variable node or $\mu_{f\to x}(x) = f(x)$ if it is a factor node. Each other node is activated when messages have arrived on all but one of the edges incident on it, and sends a message on the remaining edge.

When two messages have been passed over every edge, one in each direction, the SPA terminates and the marginal functions can be computed as

$$g_i(x_i) = \prod_{f\in\, n(x_i)} \mu_{f\to x_i}(x_i)\,.$$

The SPA can be also used when the underlying FG has cycles, leading to an iterative algorithm. In this case, the convergence to the exact marginalization is not guaranteed, and depends on the adopted schedule (that is, an order of evaluation of the messages) and on the structure of the graph. Using graphical techniques described in [4], it is always possible to eliminate the cycles in a graph, at the price of increasing the complexity of the SPA. Nevertheless, for many relevant problems characterized by FGs with cycles, the SPA was found to have good convergence proprieties and to provide a valuable alternative to the exact solution, with an excellent complexity/performance trade-off.

1.2.2 Information rate of channels with memory

We consider a time-invariant discrete-time channel with memory and we denote by $\mathbf{y} = (y_1, \cdots, y_K)$ and by $\mathbf{x} = (x_1, \cdots, x_K)$ the input and output sequences of the channel, respectively. Here we assume that the input sequence includes independent and identically distributed (i.i.d.)[2] symbols belonging to a finite alphabet. We also assume that we can define an auxiliary state sequence $\mathbf{s} = (s_1, \cdots, s_{K+1})$, whose values evolve according to a first-order Markov chain

[2] In [21] $\mathbf{x}$ is allowed to be Markovian.

over a time-invariant finite-element set. Under these assumptions we can write

$$p(\mathbf{y}, \mathbf{s}|\mathbf{x}) = P(s_1) \prod_{k=1}^{K} p(y_k, s_{k+1}|x_k, s_k)\,,$$

with $p(y_k, s_{k+1}|x_k, s_k)$ independent of k.

The aim here is to compute the IR between the input and output processes. We recall that it is possible to design communication schemes with arbitrarily low error rate only if the number of information bits transmitted per channel use does not exceed the IR [22]. For the channel considered in this section, the IR $I(X;Y)$ can be written as

$$I(X;Y) = \lim_{K\to+\infty} \frac{1}{K} \log_2 \left[\frac{p(\mathbf{y}|\mathbf{x})}{p(\mathbf{y})}\right]. \tag{1.2}$$

In many cases of interest, the analytical computation of (1.2) is unfeasible. We here describe the numerical method [19–21], which provides an accurate extimate of the actual IR. To use this simulation-based method, we first generate, according to the statistical properties of the source and the channel, a very long sequence $\mathbf{x}$, as well as the corresponding sequence $\mathbf{y}$—the meaning of "very long" is discussed in [21]. Then, the computation of $p(\mathbf{y})$ can be efficiently performed by the forward sum-product recursion of the Bahl-Cocke-Jelinek-Raviv (BCJR) algorithm [23]

$$\alpha_{k+1}(s_{k+1}) = \sum_{s_k} \sum_{x_k} \alpha_k(s_k) p(y_k, s_{k+1}|s_k, x_k) P(x_k) = p(\mathbf{y}_1^k, s_{k+1})$$

and we compute $p(\mathbf{y})$ as

$$p(\mathbf{y}) = \sum_{s_{K+1}} p(\mathbf{y}, s_{K+1}) = \sum_{s_{K+1}} \alpha_{K+1}(s_{K+1})\,.$$

To compute $p(\mathbf{y}|\mathbf{x})$ we use a modified forward recursion

$$\mu_{k+1}(s_{k+1}) = \sum_{s_k} \mu_k(s_k) p(y_k, s_{k+1}|s_k, x_k) = p(\mathbf{y}_1^k, s_{k+1}|\mathbf{x}_1^k)\,.$$

Finally, the estimate of (1.2) is obtained as

$$\hat{I}(X;Y) = \frac{1}{K}\left[\log_2 \frac{\sum_{s_{K+1}} \mu_{K+1}(s_{K+1})}{\sum_{s_{K+1}} \alpha_{K+1}(s_{K+1})}\right]. \tag{1.3}$$

In [21], a method to avoid problems of numerical stability in the computation of (1.3) is also proposed.

Chapter 2

Multiuser Receivers for FDM-CPM Systems

In this chapter, we focus on FDM systems where each user employs a CPM signal.

In Section 2.1, we describe the system model and compare, from an information-theoretic point of view, the performance of a satellite transmission scheme employing CPMs with that of a scheme employing linear modulations.

In Section 2.2, suboptimal reduced-complexity MUD schemes are extended to the FDM-CPM scenario and a new algorithm is also proposed. This new scheme is obtained by means of some graphical manipulations on the FG representing the joint a posteriori pmf of the transmitted symbols, rather than assuming the interference as Gaussian, as suggested in [15–17]. Possible extensions of the new scheme are also discussed.

In Section 2.3, we evaluate the asymptotic performance of FDM-CPM systems when multiuser detectors are employed at the receiver side by computing the achievable IR and the SE.

In Section 2.4, we consider practical SCCPM schemes employing suboptimal multiuser detectors as inner SISO detector. We analyze the convergence behavior of joint multiuser detection/decoding by means of an EXIT chart

analysis and show that the theoretical limits predicted by the information-theoretic analysis can be approached by SCCPM schemes. Multiuser processing issues are discussed in Section 2.5, where we propose reduced-complexity schemes for MUD in the presence of time-varying PN, and DA multiuser phase and frequency synchronization schemes. Finally some conclusions are drawn in Section 2.6.

2.1 System Model

We assume that the channel is shared by U independent users. Each user employs a code serially concatenated with a CPM modulator through a bit interleaver. Without loss of generality, we consider synchronous users, all employing the same modulation format, and an AWGN channel. The extension to the case of users with different modulation formats is straightforward. The cases of asynchronous users and of a channel with an unknown and possibly time-varying phase are discussed later.

The information bits $\mathbf{v}^{(u)}$ of user u, are encoded by encoder C_u into codewords $\mathbf{x}^{(u)}$, which are interleaved and mapped onto sequences of N M-ary symbols. We denote by $\alpha_n^{(u)} \in \{\pm 1, \pm 3, \cdots, \pm(M-1)\}$ the symbol transmitted by user u at discrete-time n. Moreover, $\boldsymbol{\alpha}^{(u)} = (\alpha_0^{(u)}, \ldots, \alpha_{N-1}^{(u)})^\dagger$ is the vector of the N symbols transmitted by user u and we also define $\boldsymbol{\alpha}_n = (\alpha_n^{(1)}, \ldots, \alpha_n^{(U)})^\dagger$ and $\boldsymbol{\alpha} = (\boldsymbol{\alpha}_0^\dagger, \ldots, \boldsymbol{\alpha}_{N-1}^\dagger)^\dagger$. The complex envelope of the received signal can be written as

$$r(t) = \sum_{u=1}^{U} s^{(u)}(t, \boldsymbol{\alpha}^{(u)}) \exp\{j2\pi f^{(u)} t\} + w(t)\,, \tag{2.1}$$

where $w(t)$ is a zero-mean circularly symmetric white Gaussian noise process with power spectral density (PSD) $2N_0$ (N_0 is assumed to be known at the receiver), $f^{(u)}$ is the difference between the carrier frequency of user u and the frequency assumed as reference for the computation of the complex envelope,

and $s^{(u)}(t, \boldsymbol{\alpha}^{(u)})$ is the CPM information-bearing signal of user u [24],

$$s^{(u)}(t, \boldsymbol{\alpha}^{(u)}) = \sqrt{\frac{2E_s^{(u)}}{T}} \exp\left\{ j2\pi h \sum_{n=0}^{N-1} \alpha_n^{(u)} q(t - nT) \right\}, \tag{2.2}$$

where $E_s^{(u)}$ is the energy per information symbol of user u, T the symbol interval, common to all users, $q(t)$ the *phase-smoothing response*, and $h = r/p$ the modulation index (r and p are relatively prime integers). The derivative of $q(t)$ is the so-called *frequency pulse*, of length L symbol intervals. In the generic time interval $[nT, nT + T)$, the CPM signal of user u is completely defined by symbol $\alpha_n^{(u)}$ and state $\sigma_n^{(u)} = (\omega_n^{(u)}, \phi_n^{(u)})$ [25], where

$$\omega_n^{(u)} = (\alpha_{n-1}^{(u)}, \alpha_{n-2}^{(u)}, \ldots, \alpha_{n-L+1}^{(u)}) \tag{2.3}$$

is the *correlative state* and $\phi_n^{(u)}$ is the *phase state* which can be recursively defined as

$$\phi_n^{(u)} = [\phi_{n-1}^{(u)} + \pi h \alpha_{n-L}^{(u)}]_{2\pi}, \tag{2.4}$$

where $[\cdot]_{2\pi}$ denotes the "modulo 2π" operator, and takes on p values. In the following, we define $\boldsymbol{\sigma}_n = (\sigma_n^{(1)}, \ldots, \sigma_n^{(U)})^\dagger$ and $\boldsymbol{\sigma} = (\boldsymbol{\sigma}_0^\dagger, \ldots, \boldsymbol{\sigma}_N^\dagger)^\dagger$.

Considering the useful component of the received signal (2.1), in the time interval $[nT, nT + T)$ only $(pM^L)^U$ possible waveforms are allowed. Hence, a set of sufficient statistics for detection can be obtained through projection of each slice of duration T of the received signal $r(t)$ onto an orthonormal basis, of cardinality at most M^{LU}, of the signal space of these possible waveforms. The use of an orthonormal basis ensures that the noise components are i.i.d. complex Gaussian random variables with independent components, each with mean zero and variance N_0. In practical receivers, an approximated set of sufficient statistics is obtained through the technique described in [26]. It is assumed that the useful signal component in $r(t)$ is band-limited—although this is not strictly true in the case of CPM signals, whose spectrum has an infinite support—with bandwidth lower than $\eta/2T$, where η is a proper integer. The approximated statistics can be obtained by extracting η samples per symbol

interval from the received signal prefiltered by means of an analog low-pass filter which leaves unmodified the useful signal and has a vestigial symmetry around $\eta/2T$.[1] The condition on the vestigial symmetry of the analog prefilter ensures that the noise samples are i.i.d. complex Gaussian random variables with independent components, each with mean zero and variance $\Xi^2 = N_0\eta/T$.

Although not necessary in the derivation of the algorithms, since it applies unmodified independently of the employed orthogonal basis, the only difference being the noise variance, in the following we assume a sufficient statistic obtained through oversampling. We denote by $r_{n,m}$ the m-th received sample ($m = 0, 1, \ldots, \eta - 1$) of the n-th symbol interval. It can be expressed as

$$r_{n,m} = \sum_{u=1}^{U} s_{n,m}^{(u)}(\alpha_n^{(u)}, \sigma_n^{(u)}) + w_{n,m}\,, \tag{2.5}$$

where, as mentioned, $\{w_{n,m}\}$ are i.i.d. complex Gaussian noise samples and $s_{n,m}^{(u)}(\alpha^{(u)}, \sigma^{(u)})$ (whose dependence on $\alpha^{(u)}$ and $\sigma^{(u)}$ is omitted in the following) is the contribution of user u to the useful signal component. In the following, we define $\mathbf{r}_n = (r_{n,0}, r_{n,1}, \ldots, r_{n,\eta-1})^\dagger$, $\mathbf{r} = (\mathbf{r}_0^\dagger, \mathbf{r}_1^\dagger, \ldots, \mathbf{r}_{N-1}^\dagger)^\dagger$ and $\mathbf{s}_n^{(u)} = (s_{n,0}^{(u)}, s_{n,1}^{(u)}, \ldots, s_{n,\eta-1}^{(u)})^\dagger$.

2.1.1 CPMs for satellite channels: comparison to linear modulations

CPM is appealing in satellite communications for its robustness to nonlinearities, stemming from the constant envelope, its claimed power and spectral efficiency [24, 25], and its recursive nature which allows to employ it in serially concatenated schemes [11–13].

Using information-theoretic arguments, we compare CPM-based systems with satellite transmission schemes employing linear modulations. This analysis is far form being a complete comparison since many technology and cost factors are not taken into account. The aim of this study is to motivate our

[1] This approach is equivalent of using an orthogonal basis of properly delayed sinc functions.

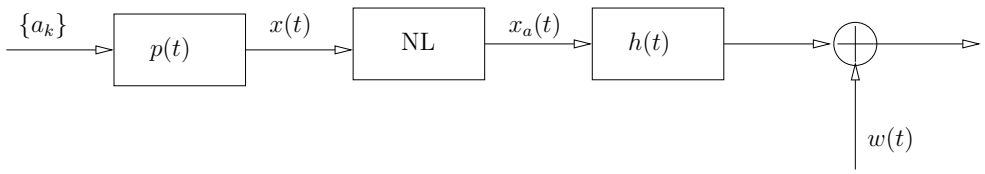

Figure 2.1: Nonlinear system.

interest in CPM schemes, showing the achievable gain in terms of SE with respect to linear modulations, considering a simplified system model.

In a typical satellite system, the transponder model is composed of an input demultiplexer filter (IMUX), a nonlinear power amplifier, and an output multiplexer filter (OMUX). Nonlinear traveling wave tube amplifiers (TWTAs) are commonly used in satellite communications. The amplifier causes phase and amplitude distortions to the transmit signal which exhibits a bandwidth expansion effect. The IMUX/OMUX filters are inserted to limit the signal bandwidth before the transmission on the physical channel and they cause linear distortions. Normally, the IMUX filter bandwidth is wider than that of the signal at its input. It is mainly the OMUX that prevents interference from adjacent transponders. In any case, the joint effect of the transmit shaping filter and that of the IMUX filter can be easily accounted for. Hence, we consider the simplifyed transmission system shown in Fig. 2.1. A sequence of M-ary complex-valued symbols $\{\alpha_k\}$ is linearly modulated obtaining the baseband signal

$$x(t) = \sum_{n=-\infty}^{\infty} \alpha_n p(t - nT)\,. \tag{2.6}$$

Symbols $\{\alpha_k\}$ and the shaping pulse $p(t)$ are properly normalized. The signal $x(t)$ is fed to the nonlinear power amplifier, which causes nonlinear distortions. Filter $h(t)$, which follows the amplifier, then limits the signal bandwidth. The signal is also corrupted by AWGN $w(t)$, with PSD $2N_0$. The resulting system is nonlinear with memory and describes a single-carrier per transponder operation.

We write the signal at the amplifier output as

$$x_a(t) = F(|x(t)|)e^{j(\angle x(t)+\Phi(|x(t)|))},$$

where $|x(t)|$ and $\angle x(t)$ are amplitude and phase of $x(t)$, respectively. Functions $F(A)$ and $\Phi(A)$ describe the amplitude (AM/AM characteristic of the amplifier) and the phase (AM/PM characteristic) distortions induced by the amplifier to a signal with given instantaneous amplitude A.

In the results we use the Saleh analytical model for the TWTA [27]. This model uses simple two-parameter functions to describe the amplitude and phase characteristics of the amplifier, and accurately matches the actual measured data for TWTAs. We consider Amplitude-Phase Shift Keying (APSK) modulations, since they are often employed in satellite systems [28] for the circular symmetry of the constellation which makes them more robust to nonlinear distortions than classical squared QAM constellations [29]. We use a double-ring 4+12-APSK, where the ratio between the two radii is 3.75 and the angle between the two rings is equal to zero. The shaping pulse $p(t)$ is a raised-cosine (RC) pulse with roll-off 0.3—values higher than 0.3 are hardly used in practice. The filter $h(t)$ is an ideal low-pass filter with bandwidth $1/T$.

At the receiver end, we consider the optimal MAP symbol detector (which can be obtained by extending the MAP sequence detector described in [30]) with a constraint on the complexity, i.e., on the channel memory accounted for. In particular, using the simulation-based method described in [21], we compute the IR achievable by a MAP symbol detector for this nonlinear system assuming that the channel memory is $2T$. This assumption, due to complexity reasons, is justified by the fact that only slight performance improvements can be obtained when using a longer channel memory at the receiver. The achievable SE in bps/Hz is then computed using the bandwidth of the filter $h(t)$ as a reference.

This analysis permits to optimize the amplifier operating point, to compare different modulation formats, or different strategies (such as predistortion versus improved detection), to optimize the spacings in case of adoption

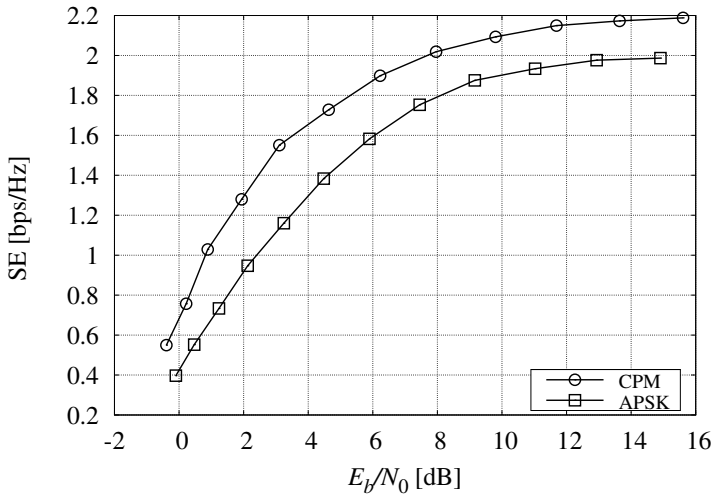

Figure 2.2: Spectral efficiency as a function of E_b/N_0, for the system with 4+12-APSK and for the system based on a quaternary CPM.

of faster-than-Nyquist signaling [31–35], to optimize the a priori probability of each modulation symbol in case of adoption of shaping [36], and so on.

When considering a satellite system employing CPMs and a single-carrier per transponder operation, we can neglect the nonlinear distortions introduced by the amplifier thanks to the constant envelope of these modulations and ignore the presence of the IMUX/OMUX filters since no bandwidth expansion is suffered by the CPM signal. To compute the SE of this transmission scheme, we use the approach suggested in [37] and define the system bandwidth as the spacing between adjacent carriers in a FDM-CPM system. We compute the IR achievable by a single-user receiver in the considered multiuser scenario, by means of the simulation-based algorithm described in [21].

In Fig. 2.2, we report the SE versus E_b/N_0, E_b being the energy per information bit, for the system with the 16-APSK modulation and for the system employing a quaternary CPM with $h = 1/6$, rectangular (REC) frequency pulse and $L = 2$. For the CPM scenario we used a normalized frequency

spacing between adjacent channels equal to 0.5. For the scheme with linear modulation, we optimized the input back-off (IBO) operating point and we set IBO= 2 dB. The figure shows the significat improvement in terms of SE achievable by using CPM signals.

2.2 Multiuser Detection Algorithms

In this section, we derive several SISO MUD algorithms for FDM-CPM systems. We firstly describe the optimal multiuser MAP symbol detector. Then, reduced-complexity MUD techniques based on SIC (e.g., see [15, 16]) from the CDMA literature are extended to the FDM-CPM scenario. We also propose a new scheme using the framework based on FGs and the SPA [4].

2.2.1 Optimal multiuser MAP symbol receiver

In Section 2.1, the m-th received sample of the n-th symbol interval was expressed as

$$r_{n,m} = \sum_{u=1}^{U} s_{n,m}^{(u)}(\alpha_n^{(u)}, \sigma_n^{(u)}) + w_{n,m}\,.$$

Assuming that the symbols of user u are independent, the pmf $P(\boldsymbol{\alpha}, \boldsymbol{\sigma}|\mathbf{r})$ factorizes as

$$P(\boldsymbol{\alpha}, \boldsymbol{\sigma}|\mathbf{r}) \propto p(\mathbf{r}|\boldsymbol{\alpha}, \boldsymbol{\sigma})\, P(\boldsymbol{\sigma}|\boldsymbol{\alpha})\, P(\boldsymbol{\alpha})\,,$$

where

$$P(\boldsymbol{\alpha}) = \prod_{n=0}^{N-1} P(\boldsymbol{\alpha}_n) \tag{2.7}$$

$$P(\boldsymbol{\sigma}|\boldsymbol{\alpha}) = P(\boldsymbol{\sigma}_0) \prod_{n=0}^{N-1} P(\boldsymbol{\sigma}_{n+1}|\boldsymbol{\sigma}_n, \boldsymbol{\alpha}_n) \tag{2.8}$$

$$p(\mathbf{r}|\boldsymbol{\alpha}, \boldsymbol{\sigma}) \propto \prod_{n=0}^{N-1} \exp\Big\{ -\frac{1}{2\Xi^2} \Big\| \mathbf{r}_n - \sum_{u=1}^{U} \mathbf{s}_n^{(u)} \Big\|^2 \Big\}\,. \tag{2.9}$$

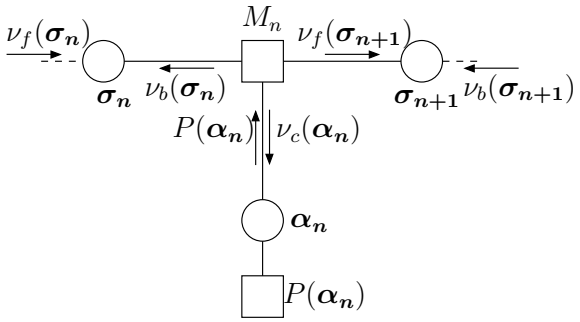

Figure 2.3: FG related to (2.10).

Notice that $P(\boldsymbol{\sigma}_{n+1}|\boldsymbol{\sigma}_n, \boldsymbol{\alpha}_n)$ is an indicator function, equal to one if $\boldsymbol{\alpha}_n$, $\boldsymbol{\sigma}_n$, and $\boldsymbol{\sigma}_{n+1}$ satisfy the trellis constraints of each user and to zero otherwise. Defining

$$M_n(\boldsymbol{\alpha}_n, \boldsymbol{\sigma}_n, \boldsymbol{\sigma}_{n+1}) = P(\boldsymbol{\sigma}_{n+1}|\boldsymbol{\sigma}_n, \boldsymbol{\alpha}_n) \exp\Big\{ -\frac{1}{2\Xi^2} \Big\| \mathbf{r}_n - \sum_{u=1}^{U} \mathbf{s}_n^{(u)} \Big\|^2 \Big\},$$

we now have

$$P(\boldsymbol{\alpha}, \boldsymbol{\sigma}|\mathbf{r}) \propto P(\boldsymbol{\sigma}_0) \prod_{n=0}^{N-1} M_n(\boldsymbol{\alpha}_n, \boldsymbol{\sigma}_n, \boldsymbol{\sigma}_{n+1}) P(\boldsymbol{\alpha}_n)\,, \tag{2.10}$$

whose corresponding FG is shown in Fig. 2.3. The SPA applied to this cycle-free FG takes the form of a forward/backward algorithm [4] (cf. Fig. 2.3 with [4, Fig. 14]), also known as BCJR algorithm [23], and provides the exact a posteriori probabilities (APPs) $P(\alpha_n^{(u)}|\mathbf{r})$. Nodes in the graph ideally become elementary processors which, according to the SPA rules, compute and exchange messages along communication channels represented by graph edges [4]. With reference to the messages represented in Fig. 2.3, by applying the SPA rules [4]

we obtain the following forward and backward recursions

$$\nu_f(\boldsymbol{\sigma}_{n+1}) = \sum_{\boldsymbol{\alpha}_n} \sum_{\boldsymbol{\sigma}_n} M_n(\boldsymbol{\alpha}_n, \boldsymbol{\sigma}_n, \boldsymbol{\sigma}_{n+1}) \nu_f(\boldsymbol{\sigma}_n) P(\boldsymbol{\alpha}_n)$$
$$\nu_b(\boldsymbol{\sigma}_n) = \sum_{\boldsymbol{\alpha}_n} \sum_{\boldsymbol{\sigma}_{n+1}} M_n(\boldsymbol{\alpha}_n, \boldsymbol{\sigma}_n, \boldsymbol{\sigma}_{n+1}) \nu_b(\boldsymbol{\sigma}_{n+1}) P(\boldsymbol{\alpha}_n)$$

with proper initial conditions [4], and the following final completion to compute the APPs

$$P(\alpha_n^{(u)}|\mathbf{r}) = P(\alpha_n^{(u)}) \nu_c(\alpha_n^{(u)})$$
$$= P(\alpha_n^{(u)}) \sum_{\boldsymbol{\sigma}_n} \sum_{\boldsymbol{\sigma}_{n+1}} M_n(\boldsymbol{\alpha}_n, \boldsymbol{\sigma}_n, \boldsymbol{\sigma}_{n+1}) \nu_f(\boldsymbol{\sigma}_n) \nu_b(\boldsymbol{\sigma}_{n+1}) \,.$$

The complexity of this optimal multiuser detector is exponential in the number of users.

2.2.2 SIC algorithms from the CDMA literature

The most efficient reduced-complexity SIC algorithm from the CDMA literature is that proposed in [15, 16] (see also [17]). It is based on a Gaussian approximation for the MAI. In other words, the algorithm can be obtained by replacing the pmf of the interfering symbols with a complex circularly symmetric Gaussian probability density function (pdf) with the same mean and variance. A SISO detector for each user is employed and they exchange soft information used to cancel out the interference.

In order to generalize the algorithm to the considered scenario, we assume that the equivalent channel for user i is

$$r_{n,m}^{(i)} = s_{n,m}^{(i)} + z_{n,m}^{(i)} \,,$$

where $z_{n,m}^{(i)}$ is the sum of interference and noise, given by

$$z_{n,m}^{(i)} = w_{n,m} + \sum_{u=1, u\neq i}^{U} s_{n,m}^{(u)} \,.$$

The vector $\mathbf{z}_n^{(i)} = (z_{n,0}^{(i)}, z_{n,1}^{(i)} \ldots, z_{n,\eta-1}^{(i)})^\dagger$, assumed to be Gaussian, has mean $\boldsymbol{\mu}_n^{(i)}$ and covariance matrix $\boldsymbol{\Phi}_n^{(i)}$ given by

$$\boldsymbol{\mu}_n^{(i)} = \sum_{u=1,u\neq i}^{U} \sum_{(\alpha_n^{(u)},\sigma_n^{(u)})} \hat{P}(\alpha_n^{(u)}, \sigma_n^{(u)}|\mathbf{r})\mathbf{s}_n^{(u)} \tag{2.11}$$

and

$$\boldsymbol{\Phi}_n^{(i)} = \sum_{u=1,u\neq i}^{U} \sum_{(\alpha_n^{(u)},\sigma_n^{(u)})} \hat{P}(\alpha_n^{(u)}, \sigma_n^{(u)}|\mathbf{r})\mathbf{s}_n^{(u)}\mathbf{s}_n^{(u)\mathrm{H}} - \boldsymbol{\mu}_n^{(i)}\boldsymbol{\mu}_n^{(i)\mathrm{H}} + 2\Xi^2\mathbf{I}\,, \tag{2.12}$$

where $\mathbf{I}$ is the identity matrix and $\hat{P}(\alpha_n^{(u)}, \sigma_n^{(u)}|\mathbf{r})$ are the estimates of the APPs provided by the SISO detector related to the interfering user u. The SISO detector for user i, in the form of a BCJR algorithm, employs Gaussian branch metrics computed from $\boldsymbol{\mu}_n^{(i)}$ and $\boldsymbol{\Phi}_n^{(i)}$ [15–17]. This suboptimal multiuser detector is then composed of U single-user detectors (SUDs) whose complexity is increased, with respect to the case when the interference is neglected, by the need to compute, for each symbol interval, $\boldsymbol{\mu}_n^{(i)}$ and $\boldsymbol{\Phi}_n^{(i)}$, through (2.11) and (2.12), to perform the inversion of $\boldsymbol{\Phi}_n^{(i)}$, and to finally compute the quadratic form in the branch metrics. In the following, this algorithm is referred to as SIC 1.

The algorithm can be simplified by neglecting the off-diagonal elements of $\boldsymbol{\Phi}_n^{(i)}$ [15]. In this way, the inversion results to be computationally less intensive at the price of a performance degradation. This simplified detector is referred to as SIC 2.

2.2.3 Proposed graph-based multiuser receiver

By using the FG/SPA framework, we now derive a new algorithm without resorting to a Gaussian approximation of the MAI. The algorithm results from a different factorization of the pmf $P(\boldsymbol{\alpha}, \boldsymbol{\sigma}|\mathbf{r})$. In fact, we can further factor-

ize (2.7), (2.8), and (2.9) as

$$\begin{aligned} P(\boldsymbol{\alpha}) &= \prod_{u=1}^{U}\prod_{n=0}^{N-1} P(\alpha_n^{(u)}) \\ P(\boldsymbol{\sigma}|\boldsymbol{\alpha}) &= \prod_{u=1}^{U} P(\sigma_0^{(u)}) \prod_{n=0}^{N-1} P(\sigma_{n+1}^{(u)}|\sigma_n^{(u)}, \alpha_n^{(u)}) \\ &= \prod_{u=1}^{U} P(\sigma_0^{(u)}) \prod_{n=0}^{N-1} I_n^{(u)}(\alpha_n^{(u)}, \sigma_n^{(u)}, \sigma_{n+1}^{(u)}) \\ p(\mathbf{r}|\boldsymbol{\alpha}, \boldsymbol{\sigma}) &\propto \prod_{n=0}^{N-1} F_n(\boldsymbol{\alpha}_n, \boldsymbol{\sigma}_n) \prod_{u=1}^{U} \mathrm{H}_n^{(u)}(\alpha_n^{(u)}, \sigma_n^{(u)}) \,, \end{aligned}$$

where

$$I_n^{(u)}(\alpha_n^{(u)}, \sigma_n^{(u)}, \sigma_{n+1}^{(u)}) = P(\sigma_{n+1}^{(u)}|\sigma_n^{(u)}, \alpha_n^{(u)}) \tag{2.13}$$

$$H_n^{(u)}(\alpha_n^{(u)}, \sigma_n^{(u)}) = \exp\Big\{\frac{1}{\Xi^2}\mathrm{Re}\Big[\mathbf{r}_n^{\mathrm{H}}\mathbf{s}_n^{(u)}\Big]\Big\} \tag{2.14}$$

$$F_n(\boldsymbol{\alpha}_n, \boldsymbol{\sigma}_n) = \prod_{i=1}^{U-1}\prod_{j=i+1}^{U} \exp\Big\{-\frac{1}{\Xi^2}\mathrm{Re}\Big[\mathbf{s}_n^{(i)\mathrm{H}}\mathbf{s}_n^{(j)}\Big]\Big\} \tag{2.15}$$

having discarded the terms independent of the symbols and states and taken into account that a CPM signal has a constant envelope. Hence, we finally have

$$\begin{aligned} P(\boldsymbol{\alpha}, \boldsymbol{\sigma}|\mathbf{r}) \propto \Big[\prod_{u=1}^{U} P(\sigma_0^{(u)})\Big] \prod_{n=0}^{N-1} F_n(\boldsymbol{\alpha}_n, \boldsymbol{\sigma}_n) \\ \cdot \prod_{u=1}^{U} H_n^{(u)}(\alpha_n^{(u)}, \sigma_n^{(u)}) I_n^{(u)}(\alpha_n^{(u)}, \sigma_n^{(u)}, \sigma_{n+1}^{(u)}) P(\alpha_n^{(u)}) \,. \end{aligned} \tag{2.16}$$

The resulting graph, shown in Fig. 2.4, has cycles of length four, that make unlikely the convergence of the SPA, since they are too short. We can remove these short cycles in the original graph by stretching [4] the variables $\sigma_n^{(u)}$ in $(\alpha_n^{(u)}, \sigma_n^{(u)})$. In other words, instead of representing variable $\alpha_n^{(u)}$ alone, we define a new variable given by the couple $(\alpha_n^{(u)}, \sigma_n^{(u)})$, thus allowing to remove the edges connecting node F_n with variable nodes $\sigma_n^{(u)}$ [4]. We remark here

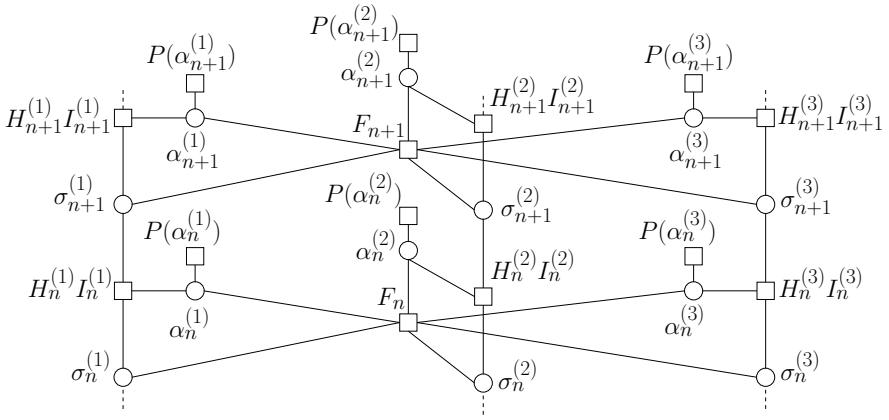

Figure 2.4: FG corresponding to (2.16) for $U = 3$.

that this transformation does not involve approximations—the resulting graph still preserves all the information of the original graph. This is not the only graph transformation that we can adopt to remove short cycles. Clustering [4] is another alternative, producing an algorithm with similar performance but slightly greater complexity.

The FG corresponding to this operation has shortest cycles of length twelve and is depicted in Fig. 2.5 in the case of a system with three users. Obviously, since cycles are still present, the SPA applied to this graph is iterative and leads to an approximate computation of the APPs $P(\alpha_n^{(u)}|\mathbf{r})$. However, the absence of short cycles allows us to obtain very good approximations, as demonstrated by the excellent performance of the algorithm.

We can introduce a further simplification, assuming that the interference among non-adjacent users is negligible. In other words, we approximate (2.15) as

$$F_n(\boldsymbol{\alpha}_n, \boldsymbol{\sigma}_n) \simeq \prod_{i=1}^{U-1} F_n^{(i,i+1)}(\alpha_n^{(i)}, \sigma_n^{(i)}, \alpha_n^{(i+1)}, \sigma_n^{(i+1)}) \,, \tag{2.17}$$

where

$$F_n^{(i,i+1)}(\alpha_n^{(i)}, \sigma_n^{(i)}, \alpha_n^{(i+1)}, \sigma_n^{(i+1)}) = \exp\Big\{ -\frac{1}{\Xi^2} \mathrm{Re}\Big[\mathbf{s}_n^{(i)\mathrm{H}} \mathbf{s}_n^{(i+1)}\Big]\Big\} \,. \tag{2.18}$$

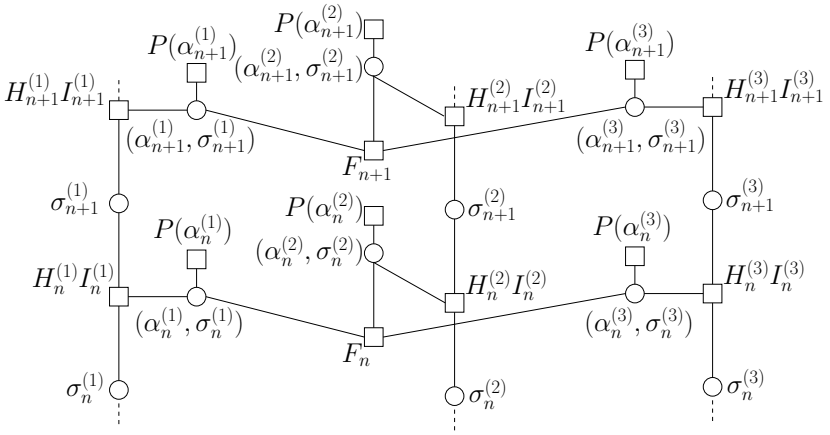

Figure 2.5: FG corresponding to (2.16) after stretching the variables $\sigma_n^{(u)}$ in $(\alpha_n^{(u)}, \sigma_n^{(u)})$ and for $U = 3$.

The corresponding FG is shown in Fig. 2.6 for $U = 3$. As the reader can observe by comparing Fig. 2.5 and Fig. 2.6, this further factorization in (2.17) implies that node F_n is split in two nodes ($U-1$ nodes, in general), $F_n^{(1,2)}$, $F_n^{(2,3)}$, each of them connecting only two adjacent users.

Let us consider the FG in Fig. 2.6. If we remove the factor nodes $F_n^{(i,i+1)}$, we obtain U SUDs which neglect the interference. Hence, these nodes are in charge of the interference mitigation. The increase in complexity due to their presence can be easily understood if we consider their role when we apply the SPA. Let us consider user i and the fact that the messages from node $(\alpha_n^{(i-1)}, \sigma_n^{(i-1)})$ to node $F_n^{(i-1,i)}$ and from node $(\alpha_n^{(i+1)}, \sigma_n^{(i+1)})$ to node $F_n^{(i,i+1)}$ have the meaning of estimates (approximations) of the APPs $P(\alpha_n^{(i-1)}, \sigma_n^{(i-1)}|\mathbf{r})$ and $P(\alpha_n^{(i+1)}, \sigma_n^{(i+1)}|\mathbf{r})$, respectively. Hence, the detector for user i employs as branch metric

$$H_n^{(i)} I_n^{(i)} P(\alpha_n^{(i)}) \sum_{(\alpha_n^{(i-1)}, \sigma_n^{(i-1)})} \hat{P}(\alpha_n^{(i-1)}, \sigma_n^{(i-1)}|\mathbf{r}) F_n^{(i-1,i)} \sum_{(\alpha_n^{(i+1)}, \sigma_n^{(i+1)})} \hat{P}(\alpha_n^{(i+1)}, \sigma_n^{(i+1)}|\mathbf{r}) F_n^{(i,i+1)} .$$

For each interfering user, the number of terms to be summed, which is related to the computational complexity, is identical to that necessary to obtain $\boldsymbol{\mu}_n^{(i)}$ or

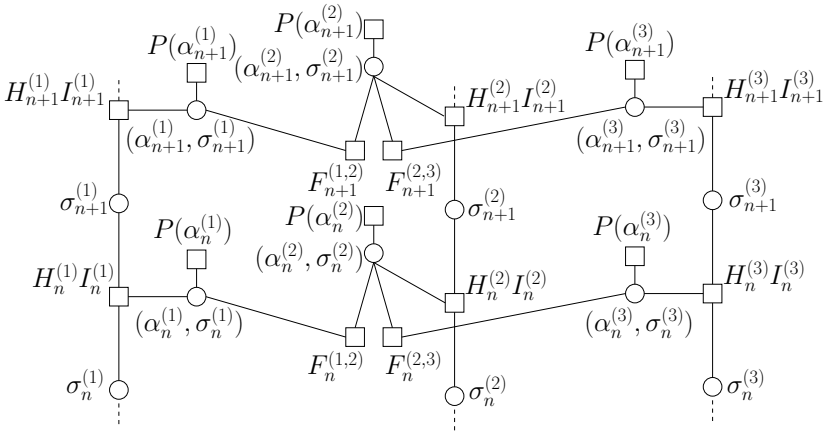

Figure 2.6: FG resulting from the approximation (2.17) and for $U = 3$.

$\mathbf{\Phi}_n^{(i)}$, through (2.11) or (2.12). However, overall, the complexity is much lower than that of SIC 1 since there is no need to compute a matrix inversion and to filter again the received vector for each iteration. The computational aspects of the described algorithms is discussed in Section 2.4.2.

As we will see in the numerical results, this new detector has a better performance than SIC 1 and SIC 2 schemes for the following reason. Since we are considering a FDM scenario, even if we increase the total number of users, there are in practice only a couple of adjacent users (or at most 4) that interfere with the considered user. As a consequence, the central limit theorem and the Gaussian approximation used to derive SIC 1 and SIC 2 schemes could not be advocated.

2.2.4 Possible extensions of the proposed algorithm

We now discuss possible extensions for the MUD algorithm proposed in the previous section.

Asynchronous signaling

The continuous-time model in (2.1) can be easily modified to account for asynchronous users by including their relative delays. The complex envelope of the received signal is now expressed by

$$r(t) = \sum_{u=1}^{U} s^{(u)}(t - \tau^{(u)}, \boldsymbol{\alpha}^{(u)}) \exp\{j2\pi f^{(u)}(t - \tau^{(u)})\} + w(t)\,,$$

where $\tau^{(u)} \in [0, T)$ is the relative time offset of user u, assumed to be known at the receiver. Without loss of generality, the smallest of these delays can be assumed to be zero. The extension of the proposed algorithm to the more general case of asynchronous users is based on the observation that, in this case, the signals of different users are not time-aligned and the interference mitigation stage involves CPM signals on two successive symbol intervals. In other words, while in the synchronous case the interference mitigation can focus on one symbol interval, the nodes $F_n^{(i,j)}$ that connect the pair of users (i, j) in the FG now depend on symbols and states of two consecutive symbol intervals. An example of FG for a system with three asynchronous users with $\tau^{(2)} = 0$ is depicted in Fig. 2.7, showing how to stretch information symbols. It has been obtained neglecting the interference among non-adjacent channels.

Laurent decomposition

Laurent decomposition [38] allows to exactly express a CPM signal as the superposition of $(M-1)2^{(L-1)\log_2 M}$ linearly modulated components. Most of the signal power is concentrated in the so-called $M-1$ *principal components*. Hence, reduced-complexity receivers can be designed starting from an approximation of a CPM signal based on these components only [9,39]. The proposed MUD algorithm can be redesigned based on an approximate CPM representation using the principal components. The algorithm is derived from the same basic ideas exploited in Section 2.2.3. In particular, we factorize the conditional pdf of the received samples highlighting the terms which take into account of the interference between adjacent channels.

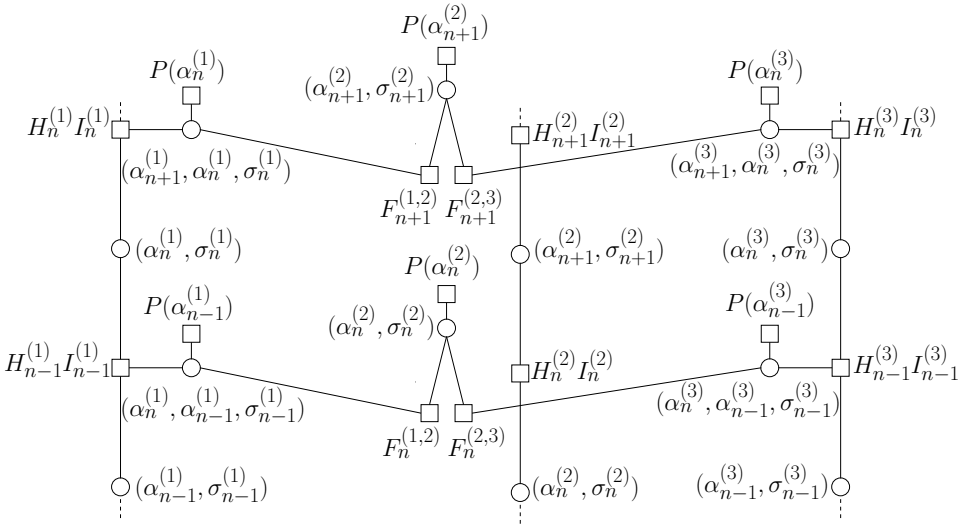

Figure 2.7: FG for three asynchronous users.

In the following this algorithm is referred to as "proposed LAU". In Section 2.2.5, we show that this approach allows to further reduce the computational complexity with a limited performance degradation.

2.2.5 Complexity considerations

We report a complexity comparison for the described reduced-complexity MUD algorithms, the O-MUD, and the SUD which simply neglects the interference. The computational complexity is assessed with reference to the coherent synchronous case. We assume that the computation of a nonlinear function is performed by using a look-up table (LUT). The number of additions between two real arguments and accesses to LUT of the considered algorithms, per user, per symbol, and per iteration, is reported in Tables 2.1 and 2.2 and refers to a logarithmic-domain implementation, which is known to provide better numerical stability and to reduce the computational complexity [40]. The operations performed only at the first iteration have been neglected (e.g. we neglect the operations for the computation of the factor nodes in the FGs of the O-MUD

Table 2.1: Number of additions per user, per symbol, per iteration.

Algorithm	Additions
Proposed	$4(pM^L)^2(U-1)+pM^L(2U+13)$ $-3pM^{L-1}-3M$
Proposed LAU	$pM(3pM-1)(2L+1)(U-1)$ $+(pM)^2+17pM-3p-3M-3$
SIC 1	$pM^L[\eta^2(3U+5)+\eta(15U-1)+18]$ $+\eta^2(8U+22)+\eta(4-4U)-3pM^{L-1}-3M$
SIC 2	$pM^L[\eta(14U-10)+18]$ $+\eta(4-4U)-3pM^{L-1}-3M$
O-MUD	$[(pM^{L-1})^U(15M^U-3)-3M^U]/U-3(M^U-M)$
SUD	$pM^{L-1}(15M-3)-3M$

and of the proposed low-complexity algorithm). For the described reduced-complexity MUD algorithms, i.e., SIC 1, SIC 2, and the proposed one, we did not exploit the following trick to further reduce the complexity. For illustration purposes, let us consider the proposed algorithm. As mentioned, it is composed by U SUDs plus the interference mitigation related to the presence of some additional nodes. When only the interference among adjacent users is accounted for and considering user u, in order to compute the function $H_n^{(u)}$ in (2.14) and functions $F_n^{(u-1,u)}$ and $F_n^{(u,u+1)}$ in (2.18), a reduced sampling frequency can be adopted, provided that the received signal is properly prefiltered, computed assuming that only users $u-1$, u, and $u+1$, are present. In this case, the number of samples per symbols, and hence the computational complexity, is reduced at the expense of an increased number of prefilters—one prefilter and a different set of samples must be used for each user.

In evaluating the complexity of SIC 1, we have considered the recursive implementation proposed in [15] for the required matrix inversion. Even with this optimization, the matrix inversion represents one of the bottlenecks of the

Table 2.2: Number of LUT accesses per user, per symbol, per iteration.

Algorithm	LUT accesses
Proposed	$(pM^L)^2(U-1)+pM^L(4-U)$ $-pM^{L-1}-M$
Proposed LAU	$pM(pM-1)(2L+1)(U-1)$ $+3pM-p-M-1$
SIC 1	$pM^L[\eta^2(4U+8)+\eta(16U-4)+3]$ $+\eta^2(13U+33)+\eta(2-2U)-pM^{L-1}-M$
SIC 2	$pM^L[\eta(15U-2)+3]$ $+\eta(2-2U)-pM^{L-1}-M$
O-MUD	$[(pM^{L-1})^U(3M^U-1)-M^U]/U+M^U-M$
SUD	$pM^{L-1}(3M-1)-M$

algorithm from a complexity viewpoint. Note that the proposed algorithm, using or not the approximate Laurent decomposition, is characterized by a complexity which increases linearly with the number of users, like SIC 2, whereas the O-MUD algorithm has a complexity which grows exponentially with U. Regarding SIC 1, its complexity seems to increase linearly with U. However, it increases quadratically with η, which in turns depends on the number of interfering users.

2.2.6 Simulation results

We report here a performance comparison for the described reduced-complexity MUD algorithms, the full-complexity O-MUD and the SUD. The O-MUD curve is a lower bound on the performance achieved by any low-complexity algorithm.

We consider SCCPM schemes with iterative decoding employing the described multiuser detectors as inner SISO detectors. In the suboptimal multiuser detectors, we can identify U SISO blocks. We distinguish between *local* iterations, within the multiuser detector, and *global* iterations, between the

multiuser detector and the U SISO decoders. In the following the possibility of executing more local iterations is not considered.

The interaction between the detector and the decoders can follow different schedules. Serial or parallel schedules are usually considered in the literature [17]. The difference in performance is practically negligible in scenarios where users transmit at the same power, and here we consider the parallel schedule, where at each iteration all the U SISO blocks in the detector are activated simultaneously. The computed soft-outputs are then provided to the SISO blocks for the other users for the next iteration round and, after deinterleaving, to the decoders. Hence a global iteration consists of a single activation of the decoders and a single local iteration of the detector. Note that the chosen schedule impacts the latency but not the complexity of the algorithms, so our computational complexity analysis is independent of this implementation aspect.

We assume that all users transmit at the same power and that channels are equally spaced in frequency. The normalized spacing is denoted by $FT = |f^{(i)} - f^{(i-1)}|T$. Each user employs a different randomly-generated bit-interleaver and Gray mapping. The bit error rate (BER) performance for the middle user only is shown versus E_b/N_0. Through this analysis, we assume that the users are synchronous. However, we also carried out a BER analysis in the asynchronous scenario observing the same performance as for the synchronous case.

In Fig. 2.8, we consider the concatenation of an outer non-recursive rate-1/2 convolutional code with generator polynomials $(5, 7)$ (in octal notation) and a quaternary modulation with $h = 1/4$ and a RC frequency pulse of duration $2T$ (2-RC). An interleaver of length 2048 bits is used and a maximum of 20 iterations is allowed. We assume that $U = 3$ users transmit simultaneously with a normalized spacing $FT = 0.55$. We consider an oversampling factor $\eta = 6$, since we found no improvement when considering higher values. From Fig. 2.8 it can be observed that the proposed algorithm achieves the best performance among suboptimal receivers. In particular, at a BER of 10^{-3} the

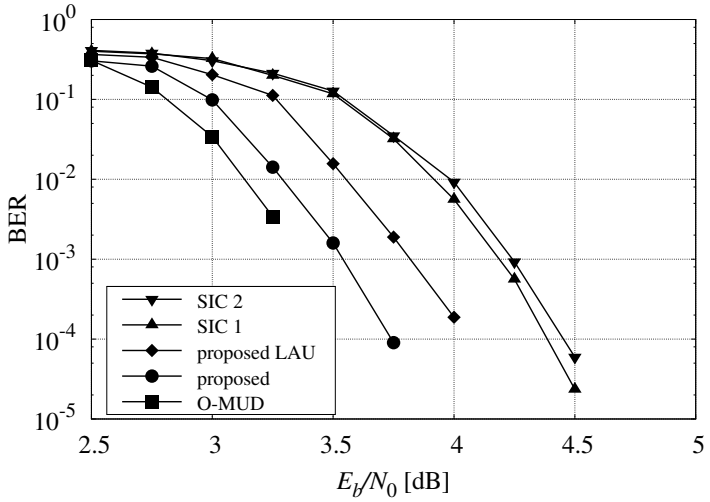

Figure 2.8: Non-recursive rate-1/2 convolutional code with generators $(5, 7)$ concatenated (through an interleaver of length 2048 bits) with a quaternary 2RC modulation with $h = 1/4$. System with $U = 3$ and a channel spacing $FT = 0.55$.

proposed algorithm gains about 0.7 dB with respect to SIC 1 and 0.8 dB with respect to SIC 2. Moreover, the loss of the proposed algorithm with respect to the O-MUD is about 0.15 dB. The loss of the proposed LAU algorithm with respect to the O-MUD is 0.4 dB. A SUD which neglects the interference is practically useless.

In Table 2.3, we show the computational complexity of the considered algorithms in the same scenario of Fig. 2.8. This table clearly shows that the proposed algorithm has a complexity much lower than that of O-MUD and SIC 1 algorithms. Interestingly, the algorithm based on the approximate Laurent representation leads to a further reduction in complexity at a price of a limited performance degradation.

In Fig 2.9, we consider the concatenation of an outer non-recursive rate-1/2 convolutional code with generators $(5, 7)$ and a minimum shift keying (MSK)

Table 2.3: Computational load per user, per symbol, per iteration for the scenario considered in Fig. 2.14.

Algorithm	Additions	LUT accesses
Proposed	33924	8236
Proposed LAU	8021	2439
SIC 1	51852	65716
SIC 2	13332	16660
O-MUD	1306380	260817
SUD	900	172

modulation, i.e., a binary modulation with $h = 1/2$ and a REC frequency pulse of duration T (1-REC). An interleaver of length 2048 bits is used and a maximum of 15 iterations is allowed. The SIC 1 scheme and the proposed algorithm described in Section 2.2.3 are considered for $U = 3$, 5, 7, and 9 and a normalized channel spacing $F = 0.5$. As expected, in both cases the performance degrades when the number of users increases—the case of $U = 3$ is obviously the most favourable one sice the side users are less subject to interference, can be detected with larger reliability, and their effect can be better mitigated on the central user of interest. We may observe that the performance advantage of the algorithm in Section 2.2.3 increases with U. This confirms what claimed before—the Gaussian approximation hardly fits the considered scenario.

2.3 Information-Theoretic Analysis

We evaluate the ultimate performance limits of FDM-CPM systems and the optimal spacing between adjacent channels by extending the analysis described in [37] to MUD strategies.

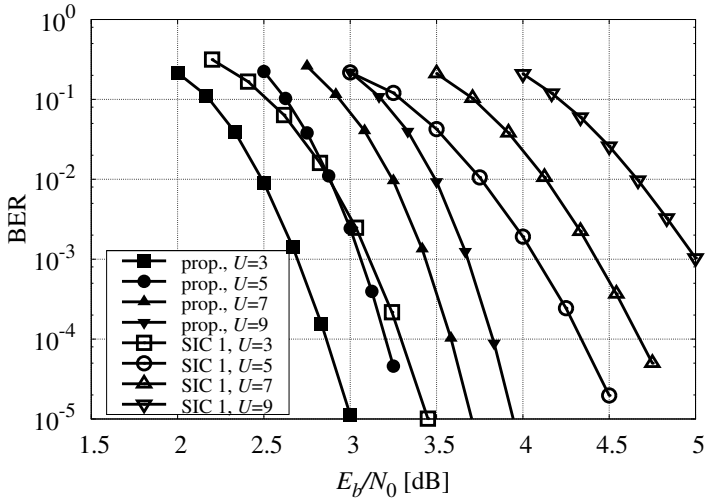

Figure 2.9: Non-recursive rate-1/2 convolutional code with generators $(5, 7)$ concatenated (through an interleaver of length 2048 bits) with the MSK modulation. Channel spacing $FT = 0.5$ and different number of users.

2.3.1 Maximization of the spectral efficiency

We assume that all users transmit at the same power ($E_s^{(u)} = E_s, u = 1, \ldots, U$), employ the same modulation format and are equally spaced in frequency. Under these conditions, the frequency spacing is a measure of the signal bandwidth and the SE can thus be computed. In order to avoid boundary effects, we assume $U \to \infty$. However, for complexity reasons we consider a multiuser detector that assumes the presence of only U' users and treats the other remaining users as additional noise. In other words, the channel model assumed by the receiver is

$$r(t) = \sum_{u=1}^{U'} s^{(u)}(t, \boldsymbol{\alpha}^{(u)}) \exp\{j2\pi f^{(u)} t\} + n(t)\,, \tag{2.19}$$

where $n(t)$ is a zero-mean circularly symmetric white Gaussian process with PSD $2(N_0 + N_I)$, N_I being a design parameter which is optimized through

computer simulations [37].

Notice that the goal here is to evaluate the ultimate performance limits achievable by a receiver designed for the auxiliary channel (2.19) when the actual channel is that in (2.1) with $U \to \infty$. This problem is an instance of mismatched decoding [41], and can be solved by means of the simulation-based method described in [21]. The method in [21] requires the existence of an algorithm for exact MAP symbol detection over the auxiliary channel (the optimal multiuser MAP symbol detector for U' users over AWGN channel described in Section 2.2.1).

We first compute the information rate for user u as

$$I(\boldsymbol{\alpha}^{(u)};\mathbf{r}) = \lim_{N\to\infty} \frac{1}{N} E\left\{ \log \frac{p(\mathbf{r}|\boldsymbol{\alpha}^{(u)})}{p(\mathbf{r})} \right\} \quad \left[\frac{\text{b}}{\text{ch. use}}\right]. \tag{2.20}$$

The pdfs $p(\mathbf{r}|\boldsymbol{\alpha}^{(u)})$ and $p(\mathbf{r})$ can be computed by a forward recursion of the optimal multiuser MAP symbol detector [21]. In (2.20), the expectation is with respect to the input and output sequences generated according to the model in (2.1). Assuming a system with an infinite number of users, the IR in (2.20) does not depend on u. Moreover, we can define the system bandwidth as the separation between adjacent channels $F = |f^{(i)} - f^{(i-1)}|$ and use it in the definition of the achievable SE

$$\text{SE} = \frac{1}{FT} I(\boldsymbol{\alpha}^{(u)};\mathbf{r}) \quad [\text{bps/Hz}]\,. \tag{2.21}$$

We remark that the use of the optimal multiuser detector for U' users is necessary to obtain achievable lower bounds on IR and SE. On the other hand, since this optimal multiuser receiver is not interesting for a complexity point of view, in the design of practical schemes in Section 2.4 we consider suboptimal reduced-complexity algorithms but using the most efficient modulation formats and the optimized spacings. The numerical results show that spacings, modulation formats, and values of SEs obtained from the information-theoretic analysis still represent a very good guideline for the design of practical systems. Obviously, some (limited) degradation must be expected.

2.3.2 Numerical results

We limit our investigation to binary and quaternary CPM formats. This choice is justified by the need to illustrate the relevant concepts and by the results which show that we can design transmission schemes with very high SE using simple CPMs. We consider binary CPMs with $h = 1/3$, $L = 2$, and REC (B-REC) or RC (B-RC) frequency pulse. Moreover we consider two quaternary formats with $h = 1/4$, $L = 2$, and REC (Q-REC) or RC (Q-RC) frequency pulse. These schemes turned out to be the best ones among those considered.

Fig. 2.10 shows the SE as a function of the spacing F for the considered CPM formats and a given value of E_s/N_0—we noticed that the optimal spacing only slightly depends on the considered value of E_s/N_0. In particular, we computed the achievable SE when a multiuser detector for different values of U' is employed. The curves with $U' = 1$ refer to the use of a SUD. For the binary CPM schemes, we also evaluated the optimal spacing when a detector with $U' = 3$ is employed; however, the curves are not plotted for the sake of clarity. The optimal spacing and the resulting SE are reported in Table 2.4 for all formats and $U' = 1, 3, 5$. For each considered CPM scheme, the MUD strategy allows to achieve a higher SE than that achievable by the SUD. Also, the frequency spacing which maximizes the SE is lower in the MUD case.

From Fig. 2.10, we can also observe that schemes with REC frequency pulse achieve higher SEs than the RC-based counterparts. The same conclusion can be drawn from Fig. 2.11, where we consider the binary CPM schemes with channel spacings resulting from the previous optimization, and we plot the SE as a function of E_b/N_0. The figure shows that REC and RC formats perform similarly for low values of SE. However, REC allows achieving a higher SE.

2.4 Practical Coding Schemes

In this section, we consider the design of practical SCCPM schemes, where the CPM modulator is concatenated with an outer code through random interleavers. The O-MUD required to compute the IR and the SE of FDM-CPM

Table 2.4: Optimal spacings and corresponding SE levels.

	U'	SE (bps/Hz)	FT
B-REC	1	1.9	0.4
	3	2.7	0.3
	5	2.9	0.3
B-RC	1	1.8	0.4
	3	2.4	0.375
	5	2.7	0.35
Q-REC	1	2.2	0.7
	3	2.9	0.6
Q-RC	1	2.0	0.7
	3	2.6	0.8

schemes is prohibitively complex for practical purposes, hence the suboptimal multiuser detector described in Section 2.2.3 is used at the destination. We analyze the convergence behavior of the proposed multiuser SCCPM schemes by means of an EXIT chart analysis [42]. The aim is to evaluate the convergence behavior of different joint decoding/detection schemes, and to assess the tradeoff between high SE and actual performance.

2.4.1 EXIT chart analysis

The joint decoding/detection scheme consists of U' APP decoders $\mathcal{C}_1^{-1}, \ldots, \mathcal{C}_{U'}^{-1}$ matched to encoders $\mathcal{C}_1, \ldots, \mathcal{C}_{U'}$ of the U' users, and a multiuser detector module $\mathcal{C}_{\mathrm{MU}}^{-1}$ consisting of U' SISO blocks (one for each user, see Section 2.2.3) to separate signals from different users. The U' SISO blocks within the multiuser detector exchange soft information among each other as well as with the U' decoders $\mathcal{C}_1^{-1}, \ldots, \mathcal{C}_{U'}^{-1}$, in an iterative fashion.

Accordingly to the chosen schedule, the iterative decoding process can be tracked using a multi-dimensional EXIT chart. Alternatively, the EXIT func-

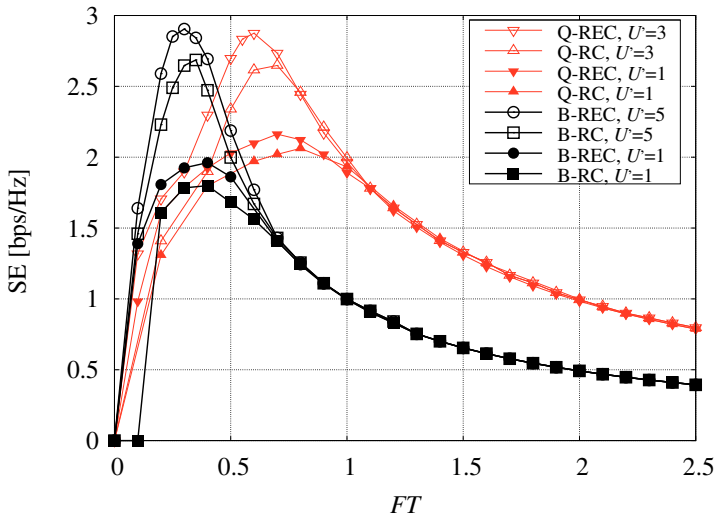

Figure 2.10: Spectral efficiency as a function of the normalized spacing for different values of U'. In the binary case $E_s/N_0 = 10$ dB, in the quaternary case $E_s/N_0 = 12$ dB.

tions of the constituent decoders and of the multiuser detector can be properly combined and projected into a two-dimensional chart [43].

Let $I^{\mathcal{C}_j}_{e,\mathbf{x}^{(j)}}$ denote the extrinsic mutual information (MI) generated by decoder $\mathcal{C}_j^{-1}$ of user j on codeword $\mathbf{x}^{(j)}$ at the output of $\mathcal{C}_j$. Also, let $I^{\mathcal{C}_{\mathrm{MU}}}_{e,\mathbf{x}^{(j)}}$ be the extrinsic MI generated by the multiuser detector on codeword $\mathbf{x}^{(j)}$ (more precisely on its interleaved version). Correspondingly, denote by $I^{\mathcal{C}_j}_{a,\mathbf{x}^{(j)}}$ and $I^{\mathcal{C}_{\mathrm{MU}}}_{a,\mathbf{x}^{(j)}}$ the *a priori* MI at the input of decoder $\mathcal{C}_j^{-1}$ and of $\mathcal{C}_{\mathrm{MU}}^{-1}$, respectively. $I^{\mathcal{C}_j}_{e,\mathbf{x}^{(j)}}$ is a function of $I^{\mathcal{C}_j}_{a,\mathbf{x}^{(j)}}$, while $I^{\mathcal{C}_{\mathrm{MU}}}_{e,\mathbf{x}^{(j)}}$ is a function of $I^{\mathcal{C}_{\mathrm{MU}}}_{a,\mathbf{x}^{(j)}}$ for $1 \leq j \leq U'$ and of the channel signal-to-noise ratio E_s/N_0:

$$\begin{aligned} I^{\mathcal{C}_j}_{e,\mathbf{x}^{(j)}} &= T^{\mathcal{C}_j}_x(I^{\mathcal{C}_j}_{a,\mathbf{x}^{(j)}}), \\ I^{\mathcal{C}_{\mathrm{MU}}}_{e,\mathbf{x}^{(j)}} &= T^{\mathcal{C}_{\mathrm{MU}}}_x(I^{\mathcal{C}_{\mathrm{MU}}}_{a,\mathbf{x}^{(1)}}, \ldots, I^{\mathcal{C}_{\mathrm{MU}}}_{a,\mathbf{x}^{(U')}}, E_s/N_0). \end{aligned} \tag{2.22}$$

Notice that $I^{\mathcal{C}_j}_{a,\mathbf{x}^{(j)}} = I^{\mathcal{C}_{\mathrm{MU}}}_{e,\mathbf{x}^{(j)}}$ and $I^{\mathcal{C}_{\mathrm{MU}}}_{a,\mathbf{x}^{(j)}} = I^{\mathcal{C}_j}_{e,\mathbf{x}^{(j)}}$. Combine now the EXIT func-

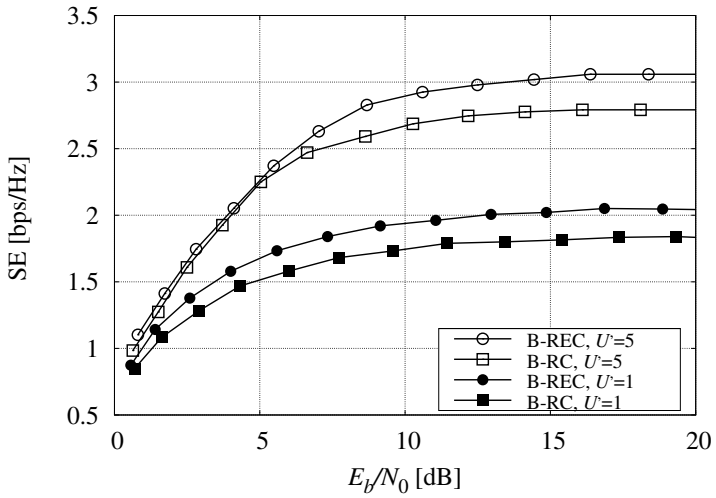

Figure 2.11: Spectral efficiency as a function of E_b/N_0, for the binary CPM schemes with channel spacings resulting from the optimization at $E_s/N_0 = 10$ dB.

tions of decoders $i \in \{1, \ldots, U'\}/j$ and of the multiuser detector in a single EXIT function, which we denote by $I^{\mathcal{C}_\mathrm{I}}_{e,\mathbf{x}^{(j)}} = T^{\mathcal{C}_\mathrm{I}}_x(I^{\mathcal{C}_\mathrm{I}}_{a,\mathbf{x}^{(j)}}, E_s/N_0)$, where $I^{\mathcal{C}_\mathrm{I}}_{a,\mathbf{x}^{(j)}} = I^{\mathcal{C}_j}_{e,\mathbf{x}^{(j)}}$. Now, the iterative process can be tracked by displaying in a single plot the EXIT function of user j, $I^{\mathcal{C}_j}_{e,\mathbf{x}^{(j)}} = T^{\mathcal{C}_j}_x(I^{\mathcal{C}_j}_{a,\mathbf{x}^{(j)}})$, and the EXIT function $I^{\mathcal{C}_\mathrm{I}}_{e,\mathbf{x}^{(j)}} = T^{\mathcal{C}_\mathrm{I}}_x(I^{\mathcal{C}_\mathrm{I}}_{a,\mathbf{x}^{(j)}}, E_s/N_0)$. $I^{\mathcal{C}_\mathrm{I}}_{e,\mathbf{x}^{(j)}}$ can be computed for all values $0 \leq I^{\mathcal{C}_\mathrm{I}}_{a,\mathbf{x}^{(j)}} \leq 1$ by activating all $U' - 1$ decoders $\mathcal{C}_1^{-1}, \ldots, \mathcal{C}_{j-1}^{-1}, \mathcal{C}_{j+1}^{-1}, \ldots, \mathcal{C}_{U'}^{-1}$ and $\mathcal{C}_\mathrm{MU}^{-1}$ until $I^{\mathcal{C}_\mathrm{I}}_{e,\mathbf{x}^{(j)}}$ has converged to a fixed value.

2.4.2 Simulation results

In the following we report a performance analysis of practical coding schemes based on serial concatenation and iterative detection/decoding. We consider scenarios with a large number of users ($U = \infty$) and a mismatched receiver designed for U' users, thus in the same conditions of the information-theoretic analysis, and also scenarios with $U = U'$ and a limited number of users. The

following results are obtained assuming synchronous users, all transmitting at the same power.

EXIT chart analysis

Here we report the numerical results obtained through the EXIT chart analysis. For each considered scheme, the channel spacing is the one obtained in Section 2.3.1. We employ a 16-state convolutional code for moderate code rates (R) and extended Bose, Ray-Chaudhuri, Hocquenghem (eBCH) codes for very high rates ($R > 0.75$) [13]. Notice that the code rate is completely determined by the SE and the (optimal) channel spacing. Gray mapping is assumed. The following results are obtained by simulating a system with a large number of users and by using a receiver working on the U' central ones. For the suboptimal detector, we carried out a coarse optimization of the noise variance to be used in the branch metrics (2.14) and (2.15).

In Fig 2.12 we plot the EXIT curves for two binary SCCPM schemes with SE= 2.33 bps/Hz and $U' = 5$. The results refer to the central user (e.g. $j = 3$ at the receiver, following the notation in Section 2.4.1). The solid curves correspond to the B-RC scheme. To obtain a SE= 2.33 bps/Hz we use a $(64, 51)$ eBCH code with $R = 0.8$. The dashed curves correspond to the B-REC scheme and a convolutional code with $R = 0.7$—we recall that the optimal spacing for the REC schemes is lower than that obtained in the RC cases. The tunnel between the two curves opens at $E_b/N_0 = 7.5$ dB for the B-RC scheme and at $E_b/N_0 = 6.4$ dB for the B-REC case, showing an improvement of about 1 dB in terms of convergence threshold if the B-REC scheme is used.

In Tables 2.5 and 2.6 we report the iterative convergence thresholds in E_b/N_0 for the central user, for binary and quaternary REC and RC SCCPM schemes for several values of the SE and $U' = 3, 5$. The corresponding code rate is also reported in the tables. For each CPM format, the highest value of SE which has been considered is slightly lower than the maximum achievable since we consider suboptimal reduced-complexity detection schemes. In the tables, we also report the achievable IR threshold in E_b/N_0 for the mismatched

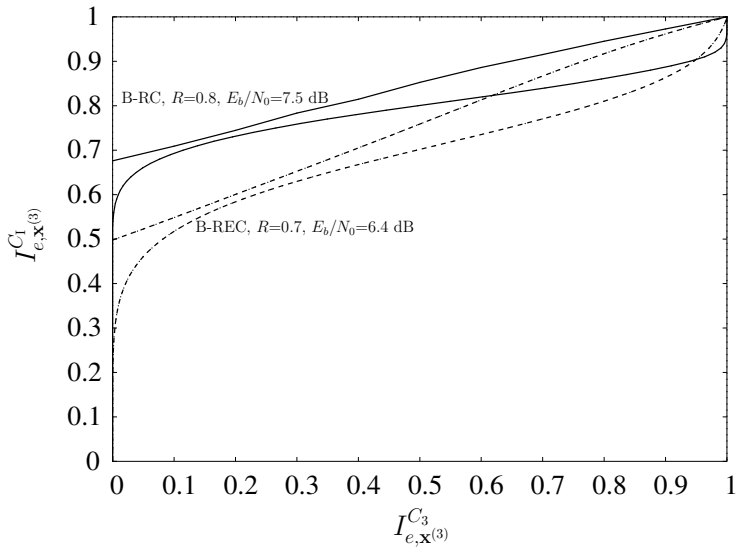

Figure 2.12: EXIT Chart for the two binary SCCPM schemes with SE=2.33 bps/Hz and $U' = 5$.

Table 2.5: Convergence threshold for the suboptimal detector versus achievable information rate for $U' = 3$

SE (bps/Hz)	Format	IR threshold $U' = 3$	Convergence threshold $U' = 3$	Gap $U' = 3$	R $U' = 3$
2	B-REC	4.8 dB	6.4 dB	1.6 dB	0.6
	B-RC	5 dB	6.4 dB	1.4 dB	0.75
2.33	B-REC	6.2 dB	8.3 dB	2.1 dB	0.7
	B-RC	9 dB	12.5 dB	3.5 dB	0.88
2.66	B-REC	10.6 dB	17.5 dB	6.9 dB	0.8
	Q-REC	8 dB	11.75 dB	3.75 dB	0.8

multiuser MAP detector obtained through the information-theoretic analysis (see Section 2.3.1).

The EXIT chart analysis confirms that REC and RC formats perform quite

Table 2.6: Convergence threshold for the suboptimal detector versus achievable information rate for $U' = 5$

SE (bps/Hz)	Format	IR threshold $U' = 5$	Convergence threshold $U' = 5$	Gap $U' = 5$	R $U' = 5$
2	B-REC	4.2 dB	5.35 dB	1.15 dB	0.6
	B-RC	4.2 dB	5.2 dB	1 dB	0.7
2.33	B-REC	5.2 dB	6.4 dB	1.2 dB	0.7
	B-RC	6 dB	7.5 dB	1.5dB	0.8
2.66	B-REC	7.6 dB	9.4 dB	1.8 dB	0.8

similarly for low SE levels and reveals that for each scheme the gap with respect to the theoretical limits is bigger for increasing values of the SE. Despite the use of a suboptimal detector, for $U' = 5$ all schemes perform between $1-1.8$ dB away from the achievable IR. From the table, we can conclude that, among the considered schemes, the best tradeoff between SE and actual performance is given by the B-REC format with $U' = 5$ and code rate $R = 0.8$.

Bit error rate performance

Here the BER results obtained through computer simulations are shown. For each scenario, we report the BER curve for the middle user. A maximum of 20 iterations between the detector and the decoders is allowed and for each user we employ a different randomly-generated bit-interleaver and Gray mapping. In Fig. 2.13, we plot the BER curve of the B-REC scheme with SE= 2.66 bps/Hz. Here, $U' = 5$, the block size for each user is of 64000 information bits and the outer code is a $(64, 51)$ eBCH code. In the figure, the achievable IR and the iterative convergence thresholds are also reported. It can be observed that the proposed scheme performs quite close to the theoretical limit, reaching a BER of 10^{-5} at $E_b/N_0 \simeq 9.6$ dB. (Notice that the multiuser detector is suboptimal). Also, the BER results are in agreement with the proposed EXIT chart analysis.

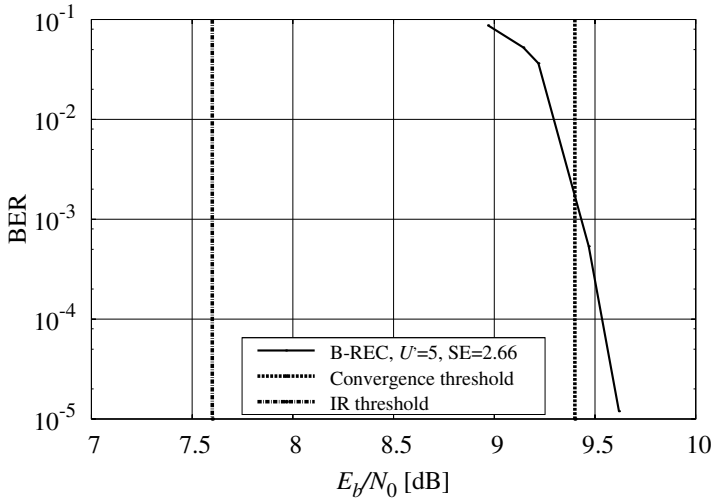

Figure 2.13: Performance and relevant thresholds for the binary, REC-based scheme with SE= 2.66 bps/Hz, 64000 information bits, $U = \infty$ and $U' = 5$.

We remark that these results can be improved through a fine optimization of the N_I parameter for the suboptimal detector.

We now consider systems with $U = U'$. In Fig 2.14, we still consider the B-REC scheme with SE= 2.66 bps/Hz, but now $U = U' = 3$ and the block size for each user is of 1024 information bits. At a BER of 10^{-3} the proposed algorithm gains about 1.1 dB with respect to SIC 1 and 1.25 dB with respect to SIC 2, and the gap increases for increasing values of E_b/N_0. The use of the approximated Laurent representation for the proposed algorithm causes a performance degradation of 0.25 dB. The loss of the proposed algorithm with respect to the O-MUD is about 0.7 dB.

The impact on the performance of the number of users is investigated in Fig. 2.15. In this figure, we assume the same system parameters as in Fig. 2.14. Only the SIC 1 scheme and the proposed algorithm described in Section 2.2.3 are considered for $U = 3$, 5, and 7. The performance advantage of the algorithm in Section 2.2.3 increases with the number of users.

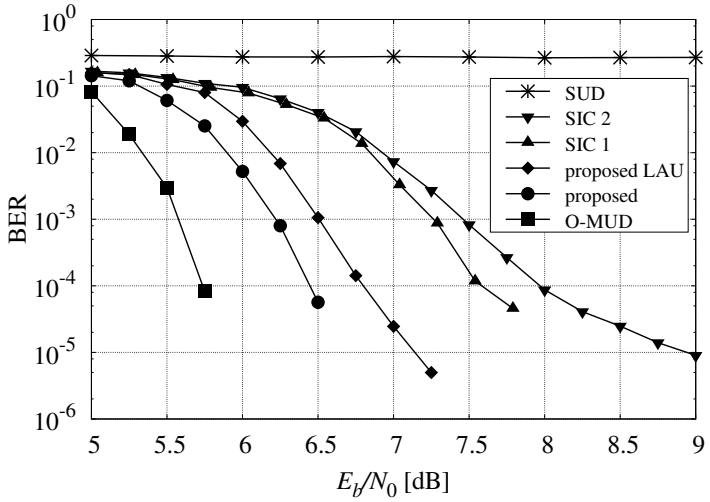

Figure 2.14: B-REC scheme with SE= 2.66 bps/Hz, 1024 information bits and $U = U' = 3$.

In Fig. 2.16, we consider the quaternary scheme with SE= 2.66 bps/Hz, namely a quaternary CPM with REC frequency pulse of length 2, $h = 1/4$, optimized channel spacing 0.6 and a $(64, 51)$ eBCH code with rate 0.8. The block size for each user is 1024. From the figure it can be observed that also in this scenario the proposed algorithm outperforms the other suboptimal receivers. At a BER of 10^{-3}, the performance gain is approximately 0.7 dB with respect to both SIC 1 and SIC 2 algorithms. Notice that as for the previous scenario, the SUD is definitely unable to manage the interference.

2.5 Carrier Synchronization Algorithms

In this Section, multiuser synchronization issues are discussed, and we propose reduced-complexity schemes for MUD in the presence of time-varying PN, and multiuser DA phase and frequency synchronization schemes.

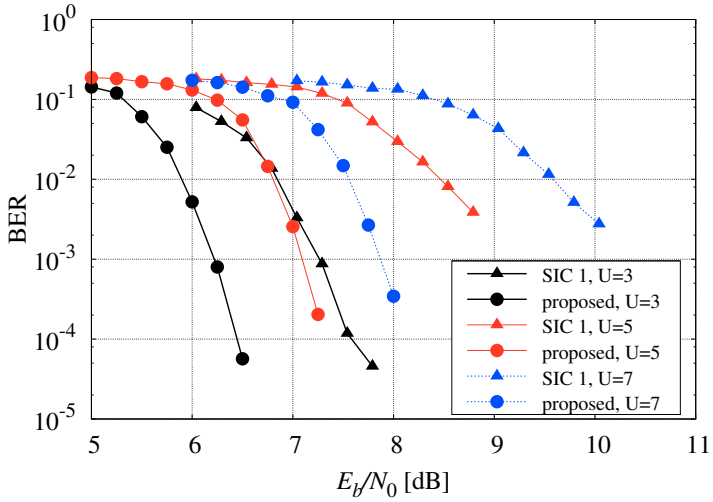

Figure 2.15: B-REC scheme with SE= 2.66 bps/Hz, 1024 information bits, $U = U'$ and different number of users.

2.5.1 Multiuser joint detection and phase synchronization

In the presence of a time-varying PN, phase synchronization must be performed jointly with detection [5,9]. For simplicity, we consider the case of synchronous users. Denoting by $\theta^{(u)}(t)$ the time-varying PN affecting the u-th signal, assumed constant over an interval of length T, the m-th received sample in the n-th symbol interval can be expressed as

$$r_{n,m} = \sum_{u=1}^{U} s_{n,m}^{(u)}(\alpha_n^{(u)}, \sigma_n^{(u)}) e^{j\theta_n^{(u)}} + w_{n,m}\,, \tag{2.23}$$

where $\theta_n^{(u)} = \theta^{(u)}(nT)$. We follow the Bayesian approach employed in [9] to design SUDs for the PN channel. The discrete-time random process $\{\theta_n{}^{(u)}\}$ is modeled according to a discrete-time Wiener process, whose incremental standard deviation over a symbol interval σ_Δ is known at the receiver [9]. We also assume that $\{\theta_n{}^{(u)}\}$ and $\{\theta_n{}^{(v)}\}$, $u \neq v$, are independent of each other.

We can rewrite the signal of user u highlighting the component that depends

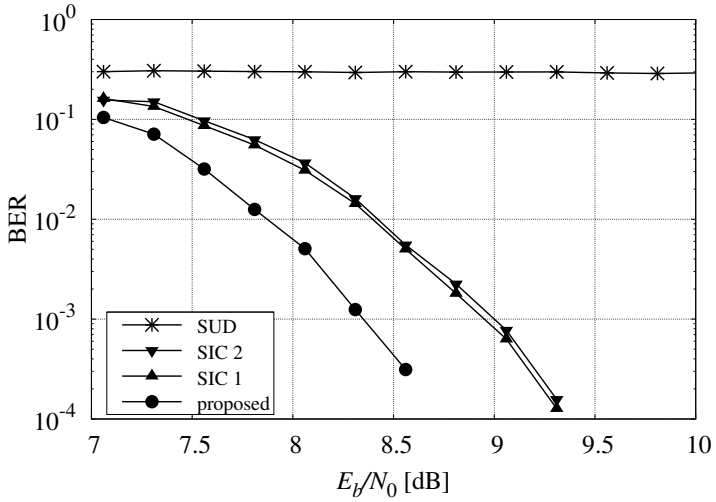

Figure 2.16: Q-REC scheme with SE= 2.66 bps/Hz, 1024 information bits and $U = U' = 3$.

on the CPM phase state:

$$s_{n,m}^{(u)}(\alpha_n^{(u)}, \sigma_n^{(u)}) = \overline{s}_{n,m}^{(u)}(\alpha_n^{(u)}, \omega_n^{(u)}) e^{\jmath\phi_n^{(u)}} .$$

Defining $\psi_n^{(u)} = [\phi_n^{(u)} + \theta_n^{(u)}]_{2\pi}$, the received signal (2.23) can be expressed as

$$r_{n,m} = \sum_{u=1}^{U} \overline{s}_{n,m}^{(u)}(\alpha_n^{(u)}, \omega_n^{(u)}) e^{\jmath\psi_n^{(u)}} + w_{n,m} . \tag{2.24}$$

We define $\boldsymbol{\omega}_n = (\omega_n^{(1)}, \ldots, \omega_n^{(U)})^\dagger$, $\boldsymbol{\omega} = (\boldsymbol{\omega}_0^\dagger, \ldots, \boldsymbol{\omega}_N^\dagger)^\dagger$, $\boldsymbol{\psi}_n = (\psi_n^{(1)}, \ldots, \psi_n^{(U)})^\dagger$, $\boldsymbol{\psi} = (\boldsymbol{\psi}_0^\dagger, \ldots, \boldsymbol{\psi}_N^\dagger)^\dagger$, and $\overline{\mathbf{s}}_n^{(u)} = (\overline{s}_{n,0}^{(u)}, \overline{s}_{n,1}^{(u)}, \ldots, \overline{s}_{n,\eta-1}^{(u)})^\dagger$. Discarding the terms independent of the symbols and states and taking into account that a CPM signal has a constant envelope, the joint distribution $p(\boldsymbol{\alpha}, \boldsymbol{\omega}, \boldsymbol{\psi}|\mathbf{r})$ can be fac-

torized as

$$p(\boldsymbol{\alpha},\boldsymbol{\omega},\boldsymbol{\psi}|\mathbf{r}) \propto \Big[\prod_{u=1}^{U} P(\omega_0^{(u)})P(\psi_0^{(u)})\Big] \prod_{n=0}^{N-1} E_n(\boldsymbol{\alpha}_n,\boldsymbol{\omega}_n,\boldsymbol{\psi}_n) \tag{2.25}$$

$$\cdot \prod_{u=1}^{U} T_n^{(u)}(\alpha_n^{(u)},\omega_n^{(u)},\psi_n^{(u)}) G_n^{(u)}(\psi_{n+1}^{(u)},\psi_n^{(u)},\omega_n^{(u)}) I_n^{(u)}(\omega_{n+1}^{(u)},\omega_n^{(u)},\alpha_n^{(u)}) P(\alpha_n^{(u)})\,, \tag{2.26}$$

where

$$\begin{aligned}
I_n^{(u)}(\omega_{n+1}^{(u)},\omega_n^{(u)},\alpha_n^{(u)}) &= P(\omega_{n+1}^{(u)}|\omega_n^{(u)},\alpha_n^{(u)}) \\
G_n^{(u)}(\psi_{n+1}^{(u)},\psi_n^{(u)},\omega_n^{(u)}) &= p(\psi_{n+1}^{(u)}|\psi_n^{(u)},\omega_n^{(u)}) \\
T_n^{(u)}(\alpha_n^{(u)},\omega_n^{(u)},\psi_n^{(u)}) &= \exp\Big\{\frac{1}{\Xi^2}\mathrm{Re}\Big[\mathbf{r}_n^{\mathrm{H}}\overline{\mathbf{s}}_n^{(u)} e^{\jmath\psi_n^{(u)}}\Big]\Big\} \\
E_n(\boldsymbol{\alpha}_n,\boldsymbol{\omega}_n,\boldsymbol{\psi}_n) &= \prod_{i=1}^{U-1}\prod_{k=i+1}^{U} \exp\Big\{-\frac{1}{\Xi^2}\mathrm{Re}\Big[\overline{\mathbf{s}}_n^{(i)\mathrm{H}}\overline{\mathbf{s}}_n^{(k)} e^{-\jmath(\psi_n^{(i)}-\psi_n^{(k)})}\Big]\Big\}\,.
\end{aligned} \tag{2.27}$$

Notice that $P(\omega_{n+1}^{(u)}|\omega_n^{(u)},\alpha_n^{(u)})$ is an indicator function, equal to one if $\alpha_n^{(u)}$, $\omega_n^{(u)}$ and $\omega_{n+1}^{(u)}$ are compatible, and to zero otherwise, and $p(\psi_{n+1}^{(u)}|\psi_n^{(u)},\omega_n^{(u)}) = p(\psi_{n+1}^{(u)}|\psi_n^{(u)},\alpha_{n-L+1}^{(u)})$ is a Gaussian pdf in $\psi_{n+1}^{(u)}$ with mean $[\psi_n^{(u)}+\pi h\alpha_{n-L+1}]_{2\pi}$ and standard deviation σ_Δ. The FG corresponding to (2.26) has cycles of length four, that we remove by clustering the variables $\omega_n^{(u)}$ and $\psi_n^{(u)}$ and then stretching them in $(\alpha_n^{(u)},\omega_n^{(u)},\psi_n^{(u)})$, obtaining a graph with shortest cycles of length twelve. Assuming as in Section 2.2.3 that the interference among non-adjacent users is negligible, we approximate (2.27) as

$$E_n(\boldsymbol{\alpha}_n,\boldsymbol{\omega}_n,\boldsymbol{\psi}_n) \simeq \prod_{i=1}^{U-1} E_n^{(i,i+1)}(\alpha_n^{(i)},\omega_n^{(i)},\psi_n^{(i)},\alpha_n^{(i+1)},\omega_n^{(i+1)},\psi_n^{(i+1)})\,, \tag{2.28}$$

where

$$\begin{aligned}
&E_n^{(i,i+1)}(\alpha_n^{(i)},\omega_n^{(i)},\psi_n^{(i)},\alpha_n^{(i+1)},\omega_n^{(i+1)},\psi_n^{(i+1)}) \\
&\qquad = \exp\Big\{-\frac{1}{\Xi^2}\mathrm{Re}\Big[\overline{\mathbf{s}}_n^{(i)\mathrm{H}}\overline{\mathbf{s}}_n^{(i+1)} e^{-\jmath(\psi_n^{(i)}-\psi_n^{(i+1)})}\Big]\Big\}\,.
\end{aligned} \tag{2.29}$$

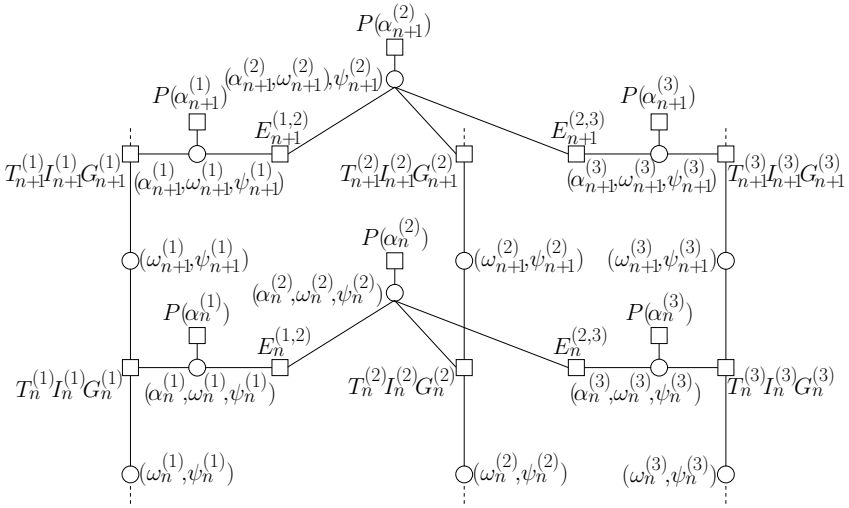

Figure 2.17: FG resulting from the approximation (2.28) and for $U = 3$.

This FG is shown in Fig. 2.17 and is similar to that for the AWGN channel (see Fig. 2.6). A major difference is represented here by the fact that continuous variables $\psi_n^{(u)}$ are now represented in the graph. Hence, the application of the SPA involves the computation of continuous pdfs and is not suited for a practical implementation. To overcome this problem, we may resort, as in [9], to the *canonical distribution* approach. Examples of commonly used canonical distributions for this channel can be found in [9]. In the numerical results, we consider a canonical distribution composed of a weighted sum of impulses. In other words, each phase $\psi_n^{(u)}$ is quantized to D equally spaced values.

Although the algorithm has been obtained by assuming a Wiener PN with known incremental variance over a symbol variance, it can be employed even when the PN follows a different model. In this case, the value of σ_Δ^2 assumed at the receiver must be optimized by simulation for the PN at hand. In any case, there is in general a benefit from using at the receiver a value of thermal noise variance σ^2 larger than the actual one. The rationale of this trick is the following: since there is an overconfidence in the computed messages, we can

make the algorithm less confident simply by describing the channel as if it added more noise than it really does [44].

2.5.2 Data-aided multiuser fine frequency synchronization

The described detection algorithms require the knowledge of the amplitude $\sqrt{2E_S/T}$ (possibly different in case of users with different powers) and frequency values $f^{(u)}$ for each user. For them, we resort to DA estimation algorithms based on known-data fields usually inserted in the frame. Amplitude estimation is not an issue here. In fact, the application of U occurrences of a DA maximum-likelihood single-user estimation algorithm provides amplitude estimates with a good accuracy for typical preamble lengths. Instead, DA single-user frequency estimation algorithms do not provide the required accuracy. This is obviously due to the interference of adjacent channels. For this reason, we employ interference cancellation to refine the estimates.

A first set of estimates of the frequency values $f^{(u)}$ is obtained by applying the DA algorithm in [45] to the preamble of each user. This algorithm does not require the knowledge of the channel phase for each user. These estimates are then iteratively refined still using the same single-user algorithm to process the received signal after the contribution of the adjacent signals has been removed. To perform interference cancellation we need to employ not only the already estimated amplitude values and the frequency values of the previous iteration, but also the instantaneous (in case of a time-varying channel phase) values of the channel phase for each user. These are obtained by using the DA multiuser carrier phase estimation algorithm described in the next section, refined every time a new set of frequency estimates becomes available.

In summary, the algorithm proceeds as follows. The amplitude of each user is estimated first. Then, at each iteration a new set of frequency estimates is derived by using the single-user DA algorithm in [45] after the contribution of adjacent users has been removed. This set of frequency estimates is employed to perform DA multiuser carrier phase estimation whose output is employed for interference cancellation at the next iteration.

A few iterations are in general sufficient, provided the known-data fields of all users have been properly optimized.

2.5.3 Data-aided multiuser carrier phase estimation

We now describe a DA multi-user carrier phase estimation algorithm that requires the knowledge of the frequency and amplitude values of each user, estimated as described in the previous section. As mentioned, the phase estimates are used for interference cancellation which is necessary to improve the frequency estimates.

Let us assume a known-data field of P symbols ($S = \eta P$ samples). Defining $z_k = r_{n,m}$, $x_k^{(u)} = s_{n,m}^{(u)}$, and $\zeta_k = w_{n,m}$, with $k = n\eta + m$, we assume that the known-data field corresponds to values $k = 0, 1, \ldots, S-1$. We also remove the hypothesis that the PN is constant over a symbol interval and define $\varphi_k^{(u)} = \theta^{(u)}(kT/\eta)$. Hence, we may express

$$z_k = \sum_{u=1}^{U} x_k^{(u)} e^{\jmath\varphi_k^{(u)}} + \zeta_k \,. \tag{2.30}$$

We define $\boldsymbol{\varphi}_k = (\varphi_k^{(1)}, \ldots, \varphi_k^{(U)})^\dagger$, $\boldsymbol{\varphi} = (\boldsymbol{\varphi}_0^\dagger, \ldots, \boldsymbol{\varphi}_{S-1}^\dagger)^\dagger$ and $\mathbf{z} = (z_0, \ldots, z_{S-1})^\dagger$. As before, we model the PN as a discrete-time Wiener process with incremental standard deviation over a symbol interval σ_Δ. We derive the MAP DA phase estimator:

$$\hat{\varphi}_k^{(u)} = \underset{\varphi_k^{(u)}}{\operatorname{argmax}}\, p(\varphi_k^{(u)}|\mathbf{z}) \qquad\qquad u = 1, \ldots, U, \quad k = 0, \ldots, S-1 \,.$$

Pdfs $p(\varphi_k^{(u)}|\mathbf{z})$ are obtained from $p(\boldsymbol{\varphi}|\mathbf{z})$ by using the FG/SPA framework. From (2.30), we may express

$$\begin{aligned} p(\boldsymbol{\varphi}|\mathbf{z}) \propto p(\mathbf{z}|\boldsymbol{\varphi})p(\boldsymbol{\varphi}) &= \prod_{k=0}^{S-1} \left[p(z_k|\boldsymbol{\varphi}_k) \prod_{u=1}^{U} p(\varphi_k^{(u)}|\varphi_{k-1}^{(u)}) \right] \\ &= \prod_{k=0}^{S-1} \left[p(z_k|\boldsymbol{\varphi}_k) \prod_{u=1}^{U} D_{k,k-1}^{(u)}(\varphi_k^{(u)} - \varphi_{k-1}^{(u)}) \right], \end{aligned} \tag{2.31}$$

where $D^{(u)}_{k,k-1}(\varphi^{(u)}_k - \varphi^{(u)}_{k-1}) = p(\varphi^{(u)}_k|\varphi^{(u)}_{k-1})$ is a Gaussian pdf with mean $\varphi^{(u)}_{k-1}$ and standard deviation $\sigma_\Delta/\sqrt{\eta}$, according to the Wiener model. Neglecting irrelevant multiplicative terms, we can further factorize

$$\begin{aligned} p(z_k|\boldsymbol{\varphi}_k) &\propto \exp\left\{-\frac{1}{2\Xi^2}\left|z_k - \sum_{u=1}^{U} x^{(u)}_k e^{\jmath\varphi^{(u)}_k}\right|^2\right\} \\ &\propto \prod_{u=1}^{U} B^{(u)}_k(\varphi^{(u)}_k) \prod_{u=1}^{U-1}\prod_{v=u+1}^{U} C^{(u,v)}_k(\varphi^{(u)}_k, \varphi^{(v)}_k) \end{aligned} \tag{2.32}$$

having defined

$$\begin{aligned} B^{(u)}_k(\varphi^{(u)}_k) &= \exp\left\{\frac{1}{\Xi^2}\mathrm{Re}\left[z_k x^{(u)*}_k e^{-\jmath\varphi^{(u)}_k}\right]\right\} \\ C^{(u,v)}_k(\varphi^{(u)}_k, \varphi^{(v)}_k) &= \exp\left\{\frac{1}{\Xi^2}\mathrm{Re}\left[x^{(u)}_k x^{(v)*}_k e^{\jmath(\varphi^{(u)}_k - \varphi^{(v)}_k)}\right]\right\}. \end{aligned}$$

From (2.31) and (2.32), we finally obtain the relevant factorization of $p(\boldsymbol{\varphi}|\mathbf{z})$. Node $C^{(u,v)}_k$ in the resulting FG connects variable nodes $\varphi^{(u)}_k$ and $\varphi^{(v)}_k$. Since the interference between two non-adjacent users is much smaller than the interference between adjacent users, we consider only functions connecting adjacent variable nodes, i.e., functions $C^{(u,u+1)}_k$. The simplified FG is shown in Fig. 2.18.

Due to the presence of cycles in the FG of Fig. 2.18, the application of the SPA gives an iterative algorithm which provides proper approximations of pdfs $p(\varphi^{(u)}_k|\mathbf{z})$. We adopt the *canonical distribution* approach and, as in [5], we model the messages represented in Fig. 2.18 as Tikhonov pdf, i.e.,

$$\begin{aligned} p^{(u)}_{f,k}(\varphi^{(u)}_k) &= t(a^{(u)}_{f,k}; \varphi^{(u)}_k) \\ p^{(u)}_{b,k}(\varphi^{(u)}_k) &= t(a^{(u)}_{b,k}; \varphi^{(u)}_k) \\ p^{(u-1,u)}_{l,k}(\varphi^{(u)}_k) &= t(a^{(u-1,u)}_{l,k}; \varphi^{(u)}_k) \\ p^{(u+1,u)}_{r,k}(\varphi^{(u)}_k) &= t(a^{(u+1,u)}_{r,k}; \varphi^{(u)}_k), \end{aligned} \tag{2.33}$$

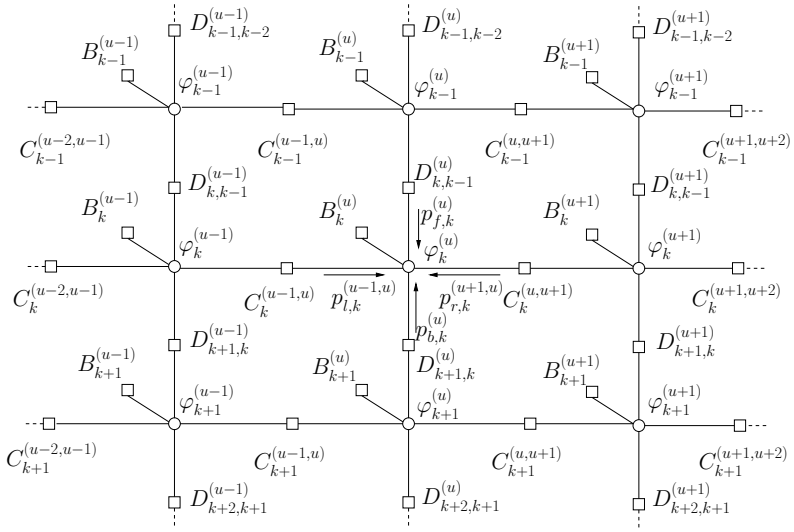

Figure 2.18: FG for the multi-user DA phase estimator.

where $t(\xi;x)$ is a Tikhonov distribution in x characterized by the complex parameter ξ:

$$t(\xi;x) = \frac{1}{2\pi \mathrm{I}_0(|\xi|)} \exp\{\mathrm{Re}[\xi e^{-jx}]\}$$

being $\mathrm{I}_0(\cdot)$ the zeroth-order modified Bessel function of the first kind. Hence, we simply have to update and propagate the complex parameters describing the Tikhonov pdfs. Let us first consider the update of parameter $a_{f,k}^{(u)}$. By generalizing the results in [5], we have

$$a_{f,k+1}^{(u)} = \gamma\Big(a_{f,k}^{(u)} + \frac{z_k x_k^{(u)*}}{\Xi^2} + a_{l,k}^{(u-1,u)} + a_{r,k}^{(u+1,u)}, \frac{\sigma_\Delta}{\sqrt{\eta}}\Big) \tag{2.34}$$

having defined

$$\gamma(\epsilon,\zeta) = \frac{\epsilon}{1+|\epsilon|\zeta^2}\,.$$

Similarly,

$$a_{b,k-1}^{(u)} = \gamma\Big(a_{b,k}^{(u)} + \frac{z_k x_k^{(u)*}}{\Xi^2} + a_{l,k}^{(u-1,u)} + a_{r,k}^{(u+1,u)}, \frac{\sigma_\Delta}{\sqrt{\eta}}\Big)\,. \tag{2.35}$$

Regarding parameters $a_{l,k}^{(u-1,u)}$ and $a_{r,k}^{(u+1,u)}$ we have

$$a_{l,k}^{(u,u+1)} = \delta\Big(a_{f,k}^{(u)} + a_{b,k}^{(u)} + \frac{z_k x_k^{(u)*}}{\Xi^2} + a_{l,k}^{(u-1,u)}, \frac{x_k^{(u)} x_k^{(u+1)*}}{\Xi^2}\Big) \tag{2.36}$$

and

$$a_{r,k}^{(u,u-1)} = \delta\Big(a_{f,k}^{(u)} + a_{b,k}^{(u)} + \frac{z_k x_k^{(u)*}}{\Xi^2} + a_{r,k}^{(u+1,u)}, \frac{x_k^{(u-1)} x_k^{(u)*}}{\Xi^2}\Big) \tag{2.37}$$

having defined

$$\delta(\epsilon, \zeta) = \frac{\epsilon\zeta}{\sqrt{|\epsilon|^2 + |\zeta|^2}}\,.$$

In order to obtain (2.36) and (2.37), two approximations have been employed: $\mathrm{I}_0(|x|) \simeq e^{|x|}$ and $\sqrt{1+x} \simeq 1 + x/2$. The following schedule is adopted: messages $a_{f,k}^{(u)}$ and $a_{b,k}^{(u)}$ are first updated, for $k = 0, \ldots, S-1$ (with initial parameter $a_{f,0}^{(u)} = 0$) and $k = S-1, \ldots, 0$ (with initial parameter $a_{b,S-1}^{(u)} = 0$), respectively. Then messages $a_{l,k}^{(u-1,u)}$ and $a_{r,k}^{(u+1,u)}$ are updated for $u = 2, \ldots, U$ and $u = U-1, \ldots, 1$, respectively. A couple of iterations are, in general, sufficient. Finally, the estimates are

$$\hat{\varphi}_k^{(u)} = \arg\left(a_{f,k}^{(u)} + a_{b,k}^{(u)} + a_{l,k}^{(u-1,u)} + a_{r,k}^{(u+1,u)} + \frac{z_k x_k^{(u)*}}{\Xi^2}\right). \tag{2.38}$$

2.5.4 Simulation results

We consider the B-REC scheme with SE= 2.66 bps/Hz and block size of 1024 information bits and a channel affected by Wiener PN with $\sigma_\Delta = 1$ degrees. In Fig. 2.19, we show the performance of the algorithm described in Section 2.5.1 and based on the discretization of the signal phase with $D = 24$ values, comparing it with that of the proposed algorithm for the AWGN channel (PN perfectly known at the receiver). For the multi-user scenario, the loss due to the PN is about 0.7 dB when $U = 3$ and 0.9 dB when $U = 5$. In the same figure we also show the curves related to a single-user scenario. In this case, the receiver for the PN channel is one of those described in [9] still working

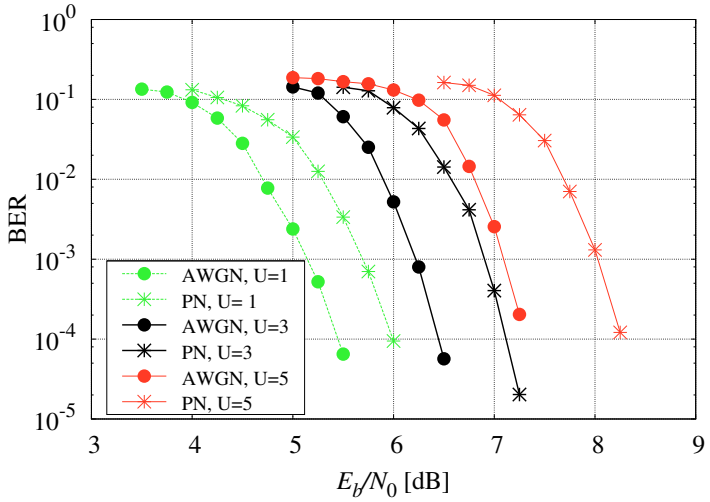

Figure 2.19: Performance of the joint detection and phase synchronization algorithm. B-REC scheme with SE= 2.66 bps/Hz. Wiener phase noise with $\sigma_\Delta = 1$ degree.

with $D = 24$ discretization levels. It is interesting to note that the loss due to the PN is approximately the same as in the multi-user scenario for $U = 3$. The loss is bigger when $U = 5$ due to the increased interference.

For the above mentioned REC-based scheme we now consider the issue of frequency synchronization. The described multiuser frequency synchronization scheme results unbiased. Hence, in Fig. 2.20 we show the mean square error (MSE) of the frequency estimate for the central user versus E_S/N_0, when $P = 60$ symbols. As a reference curve, we show the Cramér-Rao lower bound (CRB) for a system with $U = 1$, computed according to [46]. When $U = 1$, this bound is reached by the frequency estimation algorithm in [45] for $E_S/N_0 \geq$ 2 dB (curve with white circles). When $U = U' = 5$ users are present, this algorithm gives a very poor performance (curve labeled "1 iteration" since it corresponds to the first iteration of the proposed multiuser algorithm). With 4 iterations we are able to reach, for $E_S/N_0 \geq 5$ dB, the CRB related to the

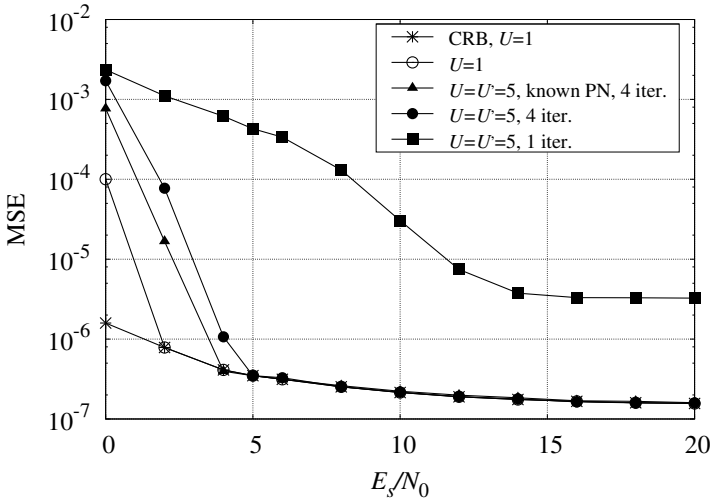

Figure 2.20: MSE of the multiuser frequency synchronization scheme in the presence of Wiener phase noise with $\sigma_\Delta = 1$ degree.

presence of only one user. Hence, a very effective interference cancellation is performed. A slightly better result is obtained by using a genie-aided version of the proposed frequency synchronization algorithm in which the true values of the channel phases are employed for interference cancellation purposes. This shows the effectiveness of the proposed DA multiuser carrier phase estimation algorithm described in Section 2.5.3.

2.6 Conclusions

In this chapter we considered FDM systems based on CPMs. We addressed the design of low-complexity suboptimal multiuser detectors and we extended to this scenario some well known MUD algorithms proposed for CDMA systems. Moreover, we introduced a new detection scheme using the framework based on FGs and the SPA. The simulation results have shown that the described algorithms allow to effectively reduce the frequency spacing between adjacent users, thus increasing the SE and in particular, it has been shown that the

new proposed graph-based detection schemes are the most effective in terms of performance and computational complexity.

These results encouraged the investigation of the ultimate performance limits of FDM-CPM systems. In particular, we optimized the channel spacing of FDM-CPM systems computing the IR and the SE. Through this analysis, we showed that it is more convenient to consider frequency spacings between the channels much lower than those usually employed to limit the interference from adjacent users, thus providing a better tradeoff between degradation of the IR due to the interference and usage of the available spectrum.

We then considered practical SCCPM schemes using the suboptimal graph-based multiuser detector at the receiver side and the optimized system parameters resulting from the theoretic study. We analyzed convergence thresholds of serially concatenated multiuser CPM through an EXIT chart analysis and showed that theoretical limits predicted by the IR analysis can be approached.

Finally we proposed reduced-complexity schemes for MUD in the presence of PN, and multiuser DA phase and frequency synchronization schemes. We showed that it is possible to implement transmission schemes with an unprecedented SE at a price of a limited complexity increase with respect to a classical single-user receiver which neglects the interference.

Chapter 3

Graph-Based Detection over Linear Channels

We consider detection over linear channels impaired by AWGN. In Section 3.1 we describe the system model. Section 3.2 introduces a few definitions and recalls some basic concepts related to MAP symbol detection for the system at hand. In Section 3.3, we present a novel FG describing the system and, by application of the SPA, we derive two SISO-detection algorithms. Section 3.4 provides some examples of channels that can be led to the considered model, discussing for each of them the complexity of the optimal MAP symbol detector. Section 3.5 reports some performance/complexity comparisons between our algorithms and some reference benchmarks. Finally, Section 3.6 concludes the chapter.

3.1 System Model

We consider linear modulations over linear channels impaired by AWGN.

In a very general form, the relationship between the transmitted sequence $\boldsymbol{c} = [c_1, c_2, \ldots, c_N]^\dagger$ and the received sequence $\boldsymbol{y} = [y_1, y_2, \ldots, y_K]^\dagger$ can be writ-

ten as [47]

$$\boldsymbol{y} = \boldsymbol{H}\boldsymbol{c} + \boldsymbol{w}\,, \tag{3.1}$$

where $\boldsymbol{w} = [w_1, w_2, \ldots, w_K]^\dagger$ are i.i.d. zero-mean Gaussian random variables, and $\boldsymbol{H}$ is a matrix with K rows and N columns. We consider the general case when all terms in (3.1) are complex-valued, assuming that the real and imaginary components of the noise samples w_i are independent and have the same variance σ^2. The model (3.1), which will be studied under the assumption of perfect knowledge of the matrix $\boldsymbol{H}$ and the variance σ^2, provides a general description for different communication schemes employing linear modulations over linear AWGN channels. For example, the matrix $\boldsymbol{H}$ can represent single- and multi-carrier transmissions over frequency-selective and possibly time-varying channels [47–49], multiple access systems [1, 3, 15–18], channels with multi-dimensional intersymbol interference (ISI) [50, 51], or even space-time architectures [52].

We are interested in MAP symbol detection [47] of the finite-order modulation symbols $\boldsymbol{c}$, given the observation of $\boldsymbol{y}$. In any system modeled by (3.1), exact MAP detection can be carried out in a simple symbol-by-symbol processing only when matrix $\boldsymbol{H}$ satisfies suitable orthogonality conditions [47]. On the other hand, in order to increase the bandwidth efficiency, it is often not convenient to pursue such orthogonality conditions in the system design [3,18,31,34]. In this case, we say that interference arises and optimal MAP detection calls for algorithms whose complexity grows exponentially with the number of interferers [47]. In most practical scenarios, such a complexity is unmanageable and suboptimal approaches are mandatory. The literature addressing low-complexity interference cancellation is huge, and an exhaustive survey is not feasible here. We focus on SIC algorithms originally proposed for CDMA systems and then extended to other applications. The reference benchmark is the algorithm proposed in [15, 16]. This algorithm was then applied in other scenarios or extended to other applications. As an example, in [1] the algorithm has been employed in FDM systems with intentional interference, in [53] has been extended to space-time architectures, and in [54, 55] has been studied for

turbo equalization [56] also investigating some approaches to further reduce the complexity. Moreover, in Chapter 2 we described the extension of the algorithm to the FDM-CPM scenario. We recall that the algorithm is founded upon the approximation of the probability distribution of the interferers as a circularly-symmetric Gaussian pdf with the same mean and variance [17]. The relevant complexity grows quadratically with the number of interferers (the number of users sharing the channel in the CDMA case) [15], which is still prohibitive in many practical scenarios. An algorithm whose complexity grows only linearly with the number of interferers is also presented in [15], but its performance is significantly worse.

3.2 Maximum-a-Posteriori Symbol Detection

We consider MAP symbol detection of symbols $\boldsymbol{c}$, which requires the evaluation of the APPs $P(c_n|\boldsymbol{y})$ for all values of n and c_n, given the observation of the received sequence $\boldsymbol{y}$. Any possible correlation between the transmitted symbols is neglected in the detection stage [55], so that the probability mass function of the transmitted sequence can be factorized as

$$P\left(\boldsymbol{c}\right) = \prod_{n=1}^{N} P_n(c_n)\,, \tag{3.2}$$

where $P_n(c_n)$ is the *a priori* probability that the symbol c_n is transmitted with index n.

The conditional pdf of the received sequence $\boldsymbol{y}$ given the modulation symbols $\boldsymbol{c}$ is

$$\begin{aligned} p(\boldsymbol{y}|\boldsymbol{c}) &= (2\pi\sigma^2)^{-K} \exp\left(-\frac{\|\boldsymbol{y}-\boldsymbol{H}\boldsymbol{c}\|^2}{2\sigma^2}\right) \\ &\propto \exp\left(-\frac{\|\boldsymbol{y}-\boldsymbol{H}\boldsymbol{c}\|^2}{2\sigma^2}\right)\,, \end{aligned} \tag{3.3}$$

the proportionality symbol $\propto$ denoting two quantities that differ by a factor

independent of $\boldsymbol{c}$, and thus irrelevant for the detection process [4]. If we define

$$\boldsymbol{x} = \boldsymbol{H}^{\mathrm{H}}\boldsymbol{y} \tag{3.4}$$

$$\boldsymbol{G} = \boldsymbol{H}^{\mathrm{H}}\boldsymbol{H}\ , \tag{3.5}$$

the 2-norm in (3.3) yields

$$\begin{aligned}\|\boldsymbol{y}-\boldsymbol{H}\boldsymbol{c}\|^2 &= \boldsymbol{y}^{\mathrm{H}}\boldsymbol{y} - 2\mathrm{Re}\{\boldsymbol{c}^{\mathrm{H}}\boldsymbol{H}^{\mathrm{H}}\boldsymbol{y}\} + \boldsymbol{c}^{\mathrm{H}}\boldsymbol{H}^{\mathrm{H}}\boldsymbol{H}\boldsymbol{c} \\ &= \boldsymbol{y}^{\mathrm{H}}\boldsymbol{y} - 2\mathrm{Re}\{\boldsymbol{c}^{\mathrm{H}}\boldsymbol{x}\} + \boldsymbol{c}^{\mathrm{H}}\boldsymbol{G}\boldsymbol{c}\ ,\end{aligned}$$

so that (3.3) can we written as

$$\begin{aligned}p(\boldsymbol{y}|\boldsymbol{c}) &\propto \exp\left(-\frac{\boldsymbol{y}^{\mathrm{H}}\boldsymbol{y} - 2\mathrm{Re}\{\boldsymbol{c}^{\mathrm{H}}\boldsymbol{x}\} + \boldsymbol{c}^{\mathrm{H}}\boldsymbol{G}\boldsymbol{c}}{2\sigma^2}\right) \\ &\propto \exp\left(\frac{2\mathrm{Re}\{\boldsymbol{c}^{\mathrm{H}}\boldsymbol{x}\} - \boldsymbol{c}^{\mathrm{H}}\boldsymbol{G}\boldsymbol{c}}{2\sigma^2}\right)\ .\end{aligned} \tag{3.6}$$

In other words, if the sequence $\boldsymbol{x}$ is available, the sequence $\boldsymbol{y}$ is irrelevant ($\boldsymbol{x}$ is a *sufficient statistic* for MAP detection [47]). Note that this was expected, since the matrix multiplication in (3.4) is actually a matched filtering [47, 57, 58]. Reminiscent of the notation used for ISI channels which, as shown in the following, is a particular case of the very general model (3.1), we call $\boldsymbol{y}$ and $\boldsymbol{x}$ as Forney's and Ungerboeck's observation models, respectively [57, 58].

The system model corresponding to (3.1) is

$$\boldsymbol{x} = \boldsymbol{H}^{\mathrm{H}}(\boldsymbol{H}\boldsymbol{c}+\boldsymbol{w}) = \boldsymbol{G}\boldsymbol{c}+\boldsymbol{\eta}\,, \tag{3.7}$$

where $\boldsymbol{\eta} = \boldsymbol{H}^{\mathrm{H}}\boldsymbol{w}$ is a sequence of circularly-symmetric Gaussian random variables, with mean zero and autocorrelation matrix $E\left[\boldsymbol{\eta}\boldsymbol{\eta}^{\mathrm{H}}\right] = 2\sigma^2\boldsymbol{G}$. It is useful to write the model in the scalar form

$$x_n = G_{n,n}c_n + \sum_{m\neq n} G_{n,m}c_m + \eta_n\ , \tag{3.8}$$

which clarifies that c_n and c_m do not interfere on each other only if the coefficient $G_{n,m} = \sum_{k=1}^{K} H_{n,k}^{*}H_{k,m}$ is null. Hence, when the matrix $\boldsymbol{G}$ is diagonal, no

interference arises, and MAP detection can be performed symbol-by-symbol. On the other hand, when $\boldsymbol{G}$ is not diagonal, the computation of the target APPs has a complexity that grows exponentially with the number of interferers [47], and is thus computationally infeasible in most practical scenarios.

Starting from model (3.1) and under the obvious assumption of zero-mean modulation symbols [47], we define the signal-to-noise ratio (SNR) as

$$\begin{aligned}\mathrm{SNR} &= \frac{E\left[||\boldsymbol{H}\boldsymbol{c}||^2\right]}{E\left[||\boldsymbol{w}||^2\right]} = \frac{E\left[\boldsymbol{c}^{\mathrm{H}}\boldsymbol{H}^{\mathrm{H}}\boldsymbol{H}\boldsymbol{c}\right]}{2\sigma^2 K} \\ &= \frac{E\left[\boldsymbol{c}^{\mathrm{H}}\boldsymbol{G}\boldsymbol{c}\right]}{2\sigma^2 K} = \frac{\sigma_c^2 \sum_{k=1}^{K} G_{k,k}}{2\sigma^2 K}\end{aligned}$$

where $\sigma_c^2 = E\{|c_m|^2\}$.

3.3 Proposed Graph-Based Detection Algorithms

In this section, we introduce a novel framework for SISO detection, obtained by applying the SPA to a FG obtained from suitable manipulations of (3.6). Let us first write the scalar forms of the matrix operations in (3.6), that is

$$\begin{aligned}\boldsymbol{c}^{\mathrm{H}}\boldsymbol{x} &= \sum_{n=1}^{N} x_n c_n^* \\ \boldsymbol{c}^{\mathrm{H}}\boldsymbol{G}\boldsymbol{c} &= \sum_{n=1}^{N} G_{n,n}|c_n|^2 + \sum_{n=1}^{N}\sum_{m<n} 2\mathrm{Re}\{G_{n,m}c_m c_n^*\}\ ,\end{aligned}$$

where the Hermitian symmetry $\boldsymbol{G} = \boldsymbol{G}^{\mathrm{H}}$, obviously implied by (3.5), was exployted. Then, we define the functions

$$T_n(c_n) = \exp\left[\frac{1}{\sigma^2}\mathrm{Re}\left\{x_n c_n^* - \frac{G_{n,n}}{2}|c_n|^2\right\}\right] \tag{3.9}$$

$$F_{n,m}(c_n, c_m) = \exp\left[-\frac{1}{\sigma^2}\mathrm{Re}\left\{G_{n,m}c_m c_n^*\right\}\right]\ , \tag{3.10}$$

so that (3.6) yields

$$p(\boldsymbol{y}|\boldsymbol{c}) \propto \prod_{n=1}^{N}\left[T_n(c_n)\prod_{m<n}F_{n,m}(c_n, c_m)\right]\ . \tag{3.11}$$

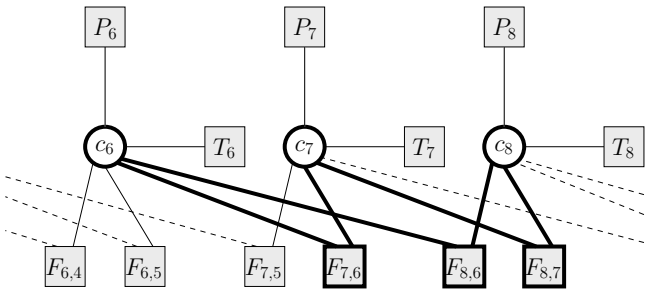

Figure 3.1: Three sections of the factor graph corresponding to (3.12), for the case when interference between c_n and c_m arises only if $|m-n| \in \{1,2\}$.

Finally, we factorize the APP of the transmitted sequence as

$$\begin{aligned} P(\boldsymbol{c}|\boldsymbol{y}) &\propto P(\boldsymbol{c})\, p(\boldsymbol{y}|\boldsymbol{c}) \\ &\propto \prod_{n=1}^{N} \left[P_n(c_n) T_n(c_n) \prod_{m<n} F_{n,m}(c_n, c_m) \right] \end{aligned} \tag{3.12}$$

by exploiting (3.2) and (3.11). Note that, when $G_{n,m} = 0$, the factor $F_{n,m}$ is equal to one and thus can be dropped from the factorization (3.12). In practice, the node $F_{n,m}$ must be included in the FG corresponding to (3.12) only when $G_{n,m} \neq 0$, i.e., only when c_n and c_m interfere on each other. An example of FG is given in Fig. 3.1. We give for understood that the node $F_{n,m}$ connecting c_n and c_m should more rigorously be denoted as the node $F_{\max\{n,m\},\min\{n,m\}}$, since the factor $F_{n,m}$ appears in (3.12) only if $n > m$. We believe that the abuse of notation is acceptable, since $F_{n,m}(c_n, c_m) = F_{m,n}(c_m, c_n)$.

We point out that the factorization (3.12) is exact, since no approximation was adopted in its derivation. On the other hand, the marginalization of (3.12) required for computing the target APPs $\{P(c_n|\boldsymbol{y})\}$ cannot be *exactly* carried out by applying the SPA to the FG in Fig. 3.1, since it contains cycles [4], as that bold-marked in the figure. It is easy to prove that the FG corresponding to (3.12) cannot contain any cycle of length lower than six, irrespectively of the number of symbols that interfere on each other. Hence, in our case, the SPA

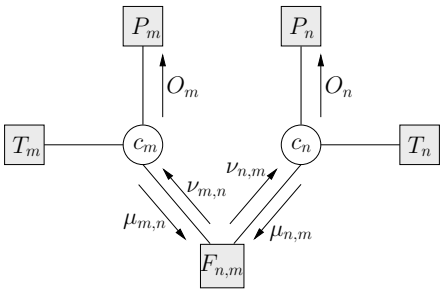

Figure 3.2: Detail of the factor graph corresponding to (3.12) and relevant notation for the propagated messages.

can be confidently adopted, since the SPA is generally expected to provide a good approximation of the exact marginalizations when the length of the cycles is at least six (see [4] for the general treatment, and [59] for an appealing application).

The algorithm resulting from the application of the SPA to the described FG has a complexity which is linear in the number of interferers. This is related to the adopted factorization having the appealing property that nodes $F_{n,m}(c_n, c_m)$, whose number linearly increases with the number of interferers, have degree two (i.e., they have two edges) irrespective of the number of interferers. A similar property is observed in some applications of detection over correlated flat-fading channels described in [7].

As shown in Fig. 3.2, we adopt the following notation for the various messages propagated over the FG:

- $O_n(c_n)$ is the message from variable node c_n to function node P_n;
- $\mu_{n,m}(c_n)$ is the message from variable node c_n to function node $F_{n,m}$;
- $\nu_{n,m}(c_n)$ is the message from function node $F_{n,m}$ to variable node c_n.

Once defined $V_n(c_n)$ as the product of all messages incoming to the variable

node c_n, namely

$$V_n(c_n) = P_n(c_n)T_n(c_n) \prod_{m \neq n} \nu_{n,m}(c_n) \ , \tag{3.13}$$

the application of the SPA leads to the following rules for message updating [4]:

$$O_n(c_n) = \frac{V_n(c_n)}{P_n(c_n)} \tag{3.14}$$

$$\mu_{n,m}(c_n) = \frac{V_n(c_n)}{\nu_{n,m}(c_n)} \tag{3.15}$$

$$\nu_{n,m}(c_n) = \sum_{c_m} F_{n,m}(c_n, c_m)\mu_{m,n}(c_m) \ . \tag{3.16}$$

All messages $\{\mu_{n,m}\}$ and $\{\nu_{n,m}\}$ should be initialized to the same positive value—the choice of this value is irrelevant [4]. Let us discuss the various messages propagated over the graph. First, we point out the probabilistic meaning of the term $V_n(c_n)$, which is proportional to the (approximated) APP $P(c_n|\boldsymbol{y})$, and that of the term $O_n(c_n)$, which is proportional to the (approximated) pdf $p(\boldsymbol{y}|c_n)$ and thus gives the so-called extrinsic information produced by the algorithm [4]. Then, the message $\nu_{n,m}(c_n)$ is proportional to the (approximated) APP of c_n, estimated locally by the node c_m [4]. Finally, the node $F_{n,m}$ just propagates (approximated) APPs between interfering nodes, after the averaging operation (3.16).

Due to the presence of cycles in the considered FG, the SPA cannot lead to a unique *schedule* nor to a unique stopping criterion for message passing [4]. Two of the various possible algorithms deriving from different schedules are described in the following—we investigated other algorithms that were found to provide improvements only in particular scenarios, and are thus not described here.

The first algorithm is referred to as *parallel-schedule* SPA (PS-SPA). It basically exploits the fact that the lower part of the FG in Fig. 3.1 is formally identical to the FG describing a low-density parity-check (LDPC) code, and adopts the same *flooding* schedule used for standard LDPC decoding [59]. The PS-SPA can be formalized by the following sequence of steps:

1. update all terms $\{V_n\}$;
2. update all messages $\{\mu_{n,m}\}$;
3. update all messages $\{\nu_{n,m}\}$;
4. if the stopping criterion is not satisfied go to step 1;
5. update all terms $\{V_n\}$.

We only consider stopping criteria based on the number of self-iterations, i.e., that is on the number of times step 4 is executed. We point out that all operations at the same step can be executed in parallel. Hence, no serial operation is required by the PS-SPA, whose latency thus does not depend on the value of N. This feature makes the PS-SPA very attractive for low-latency applications.

The second algorithm is referred to as *serial-schedule* SPA (SS-SPA), and is inspired by the *wave schedule* in [60] and by the *shuffled LDPC decoding* [61]. Let us define the *forward recursion* as the following sequence of steps, to be serially executed for each value of n from 1 to N:

a. update the messages $\{\nu_{n,m}\}_{m<n}$;

b. update the term V_n;

c. update the messages $\{\mu_{n,m}\}_{m>n}$.

Let us also define the *backward recursion* as the following sequence of steps, to be serially executed for each value of n from N down to 1:

a. update the messages $\{\nu_{n,m}\}_{m>n}$;

b. update the term V_n;

c. update the messages $\{\mu_{n,m}\}_{m<n}$.

Finally, the SS-SPA can be formalized by the following sequence of steps:

1. run the forward recursion;

2. run the backward recursion;

3. if the stopping criterion is not satisfied go to step 1.

Again, we only consider stopping criteria based on the number of self-iterations, i.e., on the number of times step 3 is executed. The SS-SPA is characterized by a latency that linearly increases with the value of N.

There exist some scenarios where both PS-SPA and SS-SPA, when implemented in the basic version described above, provide a poor performance. After deep investigations on this behavior, based on extensive computer simulations, we can state that the most significant problem is the overestimation of the reliability of the propagated messages—this is a known issue of the SPA when applied to FGs with cycles [4]. A very simple way to circumvent this problem consists of adopting in (3.9) and (3.10) a value of σ^2 larger than the actual one. The rationale of this trick is the following: since the problem is the overconfidence in the computed messages, we can make the algorithm less confident simply by describing the channel as if it added more noise than it really does. The effectiveness of this trick is proved by the simulation results reported in Section 3.5.

3.4 Examples of Channels

3.4.1 Channels with known ISI

We consider a single-carrier transmission over a channel affected by known time-invariant ISI. The continuous-time equivalent channel impulse response at the receiver is denoted by $p(t)$. Assuming ideal synchronization, at the output of a whitened matched filter the received sample at time epoch k can be expressed as [48]

$$y_k = \sum_{\ell=0}^{L_M} f_\ell c_{k-\ell} + w_k \quad , \quad k = 1, \ldots, K \tag{3.17}$$

where $c_k = 0$ for $k < 1$, L_M is the channel memory and $\{f_\ell\}_{\ell=0}^{L_M}$ is the discrete-time equivalent channel impulse response. Hence, model (3.1) holds

with $N = K$ and matrix $\boldsymbol{H}$ with entries

$$H_{m,n} = \begin{cases} f_{m-n} & \text{for } 0 \leq m-n \leq L_M \\ 0 & \text{otherwise} \end{cases} .$$

The optimal MAP symbol detection algorithm for this application is the so-called BCJR algorithm [23] whose complexity is linear in K and exponential in L_M (see also [10] for its implementation when the Ungerboeck's observation model is employed). Several algorithms have been proposed in the literature to reduce its complexity (see [6, 62] and references therein). In particular, the algorithm in [6], derived through the FG/SPA framework, has a complexity linear in K and exponential in the number of non-zero interferers, and thus is useful for sparse channels, whereas the algorithm in [62] works on the trellis describing the channel memory but explores only the most promising paths, chosen according to the MAP criterion. The SIC algorithm proposed in [15,16] can still be applied in this scenario. However, its complexity is linear in K and quadratic in L_M when the sliding window approach described in [54, 55] is adopted. An alternative approach is described in [63] based on Gaussian message passing but the complexity is still quadratic in L_M. The novel algorithm here proposed and based on the Ungerboeck's observation model, has a complexity which increases linearly with L_M.

The low-complexity algorithms for ISI channels in the literature (see [6,62] and references therein) provide a satisfactory performance when the Forney's observation model is adopted. However, for reasons discussed in [62, 64], do not result effective when the Ungerboeck's model is adopted. On the other hand, the technique proposed here works on the samples at the output of the matched filter—beside the theoretical relevance, this is of interest because the implementation of the whitening filter is critical in several practical scenarios [65].

The extension of these considerations to the case of a time-varying ISI channel is straightforward.

3.4.2 CDMA systems

The model (3.1) can describe any CDMA system observed through a linear channel with AWGN [3]. In the simplest case of a synchronous CDMA system and a non-dispersive channel, the matrix $\boldsymbol{H}$ includes the spreading sequence of the users, possibly scaled so that the different transmission powers (or the near-far effect) are properly accounted for [3]. In the more general case of an asynchronous CDMA system and/or a dispersive channel, the model (3.1) is still valid, but the expression of the matrix $\boldsymbol{H}$ is more involved [3]. For simplicity, we focus on a synchronous CDMA system impaired only by AWGN. In this case, the values of N and K represent, respectively, the number of users that share the channel and the length of the spreading sequences, measured in samples at chip rate [3], while the matching filtering (3.4) just consists of the correlation between the received signal and the spreading sequences of the users.

The complexity of the O-MUD is exponential in N [3]. We also consider two benchmark algorithms proposed in [15]. In particular, we consider the linear MMSE-based SIC described in [15–17], derived from the Gaussian approximation of the interferers and whose complexity is quadratic in N, as well as the lower-complexity version that results if the correlation between the received samples is neglected [15–17] and whose complexity in linear in N. In the following, these algorithms are referred to as SIC 1 and SIC 2, respectively. In this scenario, the complexity of the proposed algorithm is also linear in N.

3.4.3 Spectrally-efficient FDM systems

We consider an FDM system where U synchronous and independent users simultaneously access an AWGN channel transmitting at the same power—the extension to the case of asynchronous users with different power is straightforward. We assume that all users transmit the same number of symbols N_u and employ the same linear modulation format, whose corresponding base pulse is denoted by $p(t)$. We also denote by $f^{(u)}$ the difference between the carrier fre-

quency of user u and the frequency assumed as reference for the computation of the complex envelope, and by $c_n^{(u)}$ the M-ary symbol transmitted by user u at discrete-time n. Moreover, $\boldsymbol{c}^{(u)} = (c_1^{(u)}, \ldots, c_{N_u}^{(u)})^\dagger$ is the vector of the N_u symbols transmitted by user u.

A set of sufficient statistics for MAP symbol detection can be obtained through a bank of U filters matched to the pulses $p(t)e^{j2\pi f^{(u)}t}$, $u = 1, 2, \ldots, U$, and the model (3.7) holds with $N = UN_u$. The vector $\boldsymbol{c}$ contains the symbols transmitted by all users, i.e., $\boldsymbol{c} = ({\boldsymbol{c}^{(1)}}^\dagger, \ldots, {\boldsymbol{c}^{(U)}}^\dagger)^\dagger$. The matrix $\boldsymbol{G}$ is a block matrix and we denote by $\boldsymbol{G}^{(i,j)}$, $i, j = 1, \cdots, U$, the (i, j) submatrix with N_u rows and N_u columns, accounting for the correlation between users i and j. Its entries are

$$G_{n,m}^{(i,j)} = e^{j2\pi(f^{(i)}-f^{(j)})mT} \int p(t-(n-m)T)p^*(t)e^{j2\pi(f^{(i)}-f^{(j)})t}dt \qquad n, m = 1, \cdots, N_u$$

where T is the symbol period common to all users. When Nyquist pulses are employed, no ISI among symbols of the same user arises and the submatrices $\boldsymbol{G}^{(i,i)}$ are diagonal.

We consider spectrally efficient FDM transmissions, where interference among adjacent users is intentionally introduced in order to increase the bandwidth efficiency [1, 18]. In other words, the spectral efficiency is increased by reducing the spacing between two adjacent channels, allowing overlap in frequency. As a consequence, the number of non-zero off-diagonal elements in the matrix $\boldsymbol{G}$ is not negligible and multiuser detection becomes necessary [1]. The O-MUD for this scenario has a computational complexity which increases exponentially with the cardinality of the interference set. Hence, suboptimal reduced-complexity MUD techniques are required. The SIC 1 and SIC 2 algorithms, already described for CDMA systems and based on a Gaussian approximation of the MAI, can be easily extended to this scenario [1, 66, 67]. Their complexity is quadratical and linear, respectively, in the cardinality of the interference set.

The proposed algorithm has a complexity which increases linearly with the cardinality of the interference set. As we will see, this algorithm has a better performance than that of SIC 1 and SIC 2 schemes. The reason is the following. Since we are considering an FDM scenario, even if we increase the total number of users U, there are in practice only a couple of adjacent users (or at most 4) that interfere with the considered user. As a consequence, the central limit theorem and the Gaussian approximation used to derive SIC 1 and SIC 2 schemes could not be advocated.

3.4.4 Multiple-antenna channels

Model (3.1) can describe a channel with multiple transmit and receive antennas. Focusing on frequency-flat fading, K and N represent the number of receive and transmit antennas, respectively, whereas the entries of matrix $\boldsymbol{H}$ in (3.1) are the channel coefficients [52].

Computational complexity of the optimal MAP symbol detector grows exponentially with N. Many suboptimal solutions have been proposed in the literature (see [53] and references therein) all with complexity much larger than that of the proposed algorithm.

3.4.5 OFDM systems with ICI

In single-carrier communication systems, multipath channel spreads may cause severe ISI, which requires sophisticated and computationally-demanding equalization techniques. Transmission schemes based on orthogonal frequency division multiplexing (OFDM) have emerged as a more convenient solution, with the key advantage that, in time-invariant channels, modulation symbols transmitted over different subcarriers do not interfere with each other even after propagating over frequency-selective channels, so that simple symbol-by-symbol detection can be adopted [49]. Unfortunately, this property no longer holds on time-varying channels and/or in the presence of synchronization errors, as ICI arises [68]. In this case, the matrix $\boldsymbol{H}$ in (3.1) is a square matrix

where the entry $H_{m,n}$ describes the ICI between the m-th and n-th subcarriers. See [69] and references therein for an extensive survey on ICI mitigation in OFDM systems and its analogy with ISI mitigation in single-carrier systems

3.4.6 Multi-dimensional ISI channels

In the previous examples, except for the spectrally-efficient FDM systems, we have considered scenarios in which interference arises in a single domain (e.g., code domain in CDMA systems, time domain in frequency-selective ISI channels, frequency domain in OFDM systems with ICI). On the other hand, the model in (3.1) can describe more general scenarios, in which interference among the modulation symbols arises simultaneously in different domains. For example, in the case of the spectrally-efficient FDM systems described above, interference arises in the frequency domain as well as in the time domain. See also [50] and references therein for a general treatment of bidimensional ISI, and [51] for an introduction to bidimensional ISI in storage systems.

3.5 Simulation Results

The performance of the described detection schemes is here assessed by means of computer simulations. We consider coded transmissions with iterative detection/decoding at the receiver side [55]. In such systems, the MAP symbol detector is the inner SISO detection algorithm, while, according to the turbo principle [55], the terms $\{P_n\}$ (see Fig. 3.2) are iteratively updated by a SISO decoder. In the case of the SIC 1 and SIC 2 algorithms mentioned before, the terms $\{P_n\}$ are used to compute soft estimates of the transmitted symbols, which are then exploited for interference mitigation [15–17].

In the case of the proposed algorithms, extensive analyses, carried out by means of EXIT charts [70] as well as BER simulations show that it is often not convenient to execute more than one self-iteration when either the PS-SPA or the SS-SPA are employed in systems with iterative detection/decoding. Although particular scenarios were found in which self-iterations provided non

negligible gains, both algorithms typically provide a satisfactory performance when, each time the SISO decoder updates the intrinsic information $\{P_n\}$, they execute just one self-iteration before feeding out the extrinsic information $\{O_n\}$ (see Fig. 3.2). Hence, the possibility of executing more self-iterations is not discussed hereafter.

In iterative detection/decoding schemes, a further design option consists of resetting all messages in the detection FG each time the PS-SPA and the SS-SPA are fed to intrinsic information, so that any memory of the previous iterations is removed. These algorithms are referred to as PS-SPA-R and SS-SPA-R.

3.5.1 Channels with known ISI

In [71], the graph-based algorithm described in Section 3.3 has been applied to channels with known ISI. Here we summarize the performance of the proposed algorithms, implemented in the logarithmic domain [4].

All results reported in the following are related to a binary transmission with alphabet $\{\pm 1\}$ and real-valued sequences $\{f_i\}$. We consider two ISI channels, referred to as C1 and C2. Channel C1 is characterized by a shaping pulse $p(t) = p_{\mathrm{LOR}}(t) - p_{\mathrm{LOR}}(t-T)$, $p_{\mathrm{LOR}}(t)$ being a Lorentzian pulse with density $D_L = 3$ [47]—this model is commonly used for magnetic-storage systems. Channel C2 corresponds to faster-than-Nyquist signaling with roll-off equal to 0.1 and time-compression factor is 0.78 [34]—this system provides a very attractive spectral efficiency by introducing intentional ISI [34]. Both channels are characterized by an infinite value of L_M, and were truncated by setting $L_M = 12$,[1] which implies that the full-complexity forward backward algorithm (FBA) works on a 4096-state trellis. To further reduce the complexity of the PS-SPA and the SS-SPA, we neglect the coefficients $\{G_{n,m}\}$ with the lowest magnitudes. Therefore, we introduce the integer parameter $L_E \leq L_M$, and define a new FG that does not include all L_M function nodes $\{F_{n,m}\}$, but

[1] We chose L_M as the minimum integer such that $|G_{m,m-i}|/G_{m,m} < 0.01$ for all values of i larger than L_M [47].

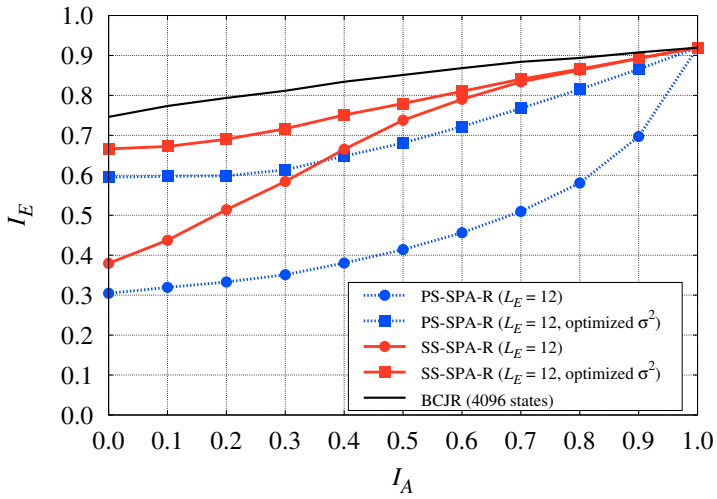

Figure 3.3: EXIT charts for different algorithms over ISI channel C1, when a binary modulation is adopted and the value of the SNR is equal to 3 dB.

only the L_E function nodes $\{F_{n,m}\}$ related to the coefficients $\{G_{n,m}\}$ with the largest magnitudes, so that the complexity is reduced by a factor L_M/L_E with respect to the original FG.

Fig. 3.3 reports EXIT charts related to transmissions over channel C1 when the value of the SNR is equal to 3 dB— see [70] for details on the EXIT charts related to detection algorithms. In Fig. 3.3, I_A and I_E denote the prior and extrinsic MI for the SISO detector. The simulations related to the PS-SPA and the SS-SPA were about 100-time faster than those related to the FBA.[2] We notice that when the assumed value of σ^2 is properly optimized, the EXIT charts of the PS-SPA and the SS-SPA significantly improve with respect to when the assumed value of σ^2 equals the actual one—in particular, σ^2 is increased by 9 dB for the PS-SPA and by 5 dB for the SS-SPA. Moreover, we notice that

[2]The PS-SPA would be even faster, but we could not implement the message passing in parallel in our simulation environment. For this reason, an implementation over Field Programmable Gate Array (FPGA) is ongoing.

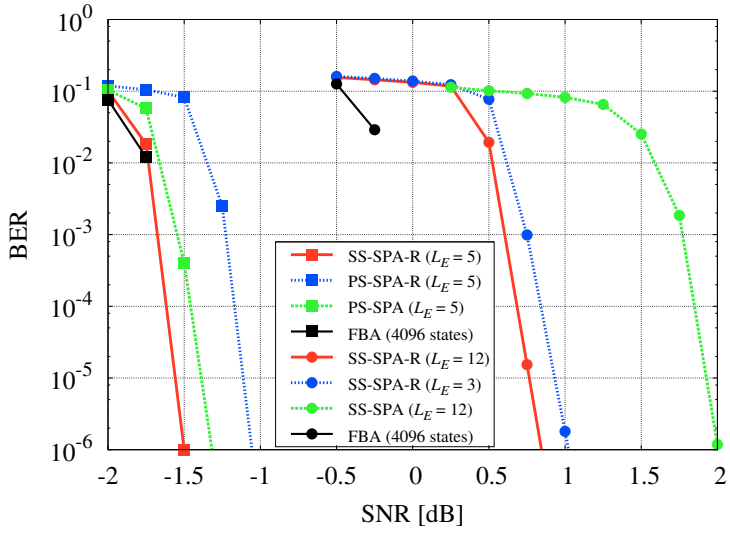

Figure 3.4: Performance over ISI channels C1 (circles) and C2 (squares). A binary modulation and an LDPC code with rate 1/2 are adopted.

the SS-SPA is noticeably more effective than the PS-SPA in this scenario, and fairly close to the performance of the optimal FBA.

Finally, in Fig. 3.4, we report the BER performance of various algorithms in a turbo equalization scheme [55, 56]. The results related to channel C1 and channel C2 are marked by circles and squares, respectively. An LDPC code with codeword length of 50,000 bits and rate 1/2 is used in both cases. A detection instance is executed before each iteration of the SISO decoder, for a maximum of 50 iterations. The process also stops if a valid codeword is found before the 50^{th} iteration. No interleaver is used because of the random nature of the LDPC code. In all cases, the algorithms are implemented after a (coarse) optimization of the assumed values of σ^2. We point out that the simulation results related to the full-complexity FBA, yet sufficient for estimating the performance loss due to the proposed algorithms, are incomplete, since it is nearly unfeasible to obtain reliable BER curves for turbo equalizers working on a 4096-state trellis. Let us notice the impressive performance of the pro-

Table 3.1: CDMA systems: Computational load per user, per symbol, per iteration, for BPSK symbols.

Algorithm	Additions	LUT accesses
Proposed	$16N - 14$	$2N - 2$
SIC 1	$2N^2 + 8N + 1$	$N^2 + 5N$
SIC 2	$9N + 2$	$6N + 2$

posed algorithms over channel C2. First, we remark that there is no need for considering more than 5 function nodes $\{H_i\}$, since the SS-SPA practically performs as the FBA when implemented with message resetting and $L_E = 5$. Then, we point out that the PS-SPA loses only few tenths of dB when implemented without message resetting and $L_E = 5$, and can be thus considered as the most convenient solution thanks to the low-latency properties discussed before. The proposed algorithms are slightly less effective over channel C1. In particular, we notice that the SS-SPA loses about 0.7 dB with respect to the FBA, but, since the simulation was about 100-time faster, this is still a very satisfactory result—to our knowledge, over this magnetic channel, the proposed solution is by far the one providing the best performance/complexity tradeoff. Fig. 3.4 also shows the impact of the value of L_E and message resetting in this scenario. Interestingly, the SS-SPA performs better when message resetting is implemented, while the PS-SPA does when message resetting is not implemented.

Other simulation results confirm the effectiveness of the proposed algorithms even when non-binary modulations and different ISI channels are considered.

3.5.2 CDMA systems

In this section, we show how the proposed SISO-detection framework can be employed in CDMA systems.

First of all, we address the computational complexity of the proposed detection algorithms, assuming binary phase shift keying (BPSK) symbols. The number of operations per user, per symbol, and per iteration of these detection algorithms are reported in Table 3.1. Note that, since the parallel/serial implementation impacts the latency but not the complexity, the table reports only one entry for both PS-SPA and SS-SPA. The reported results refer to the logarithmic-domain implementation of the algorithms, which is known to provide better numerical stability and to reduce the computational complexity [72]. The evaluation of a non linear function is counted as an access to a LUT. Note that the proposed algorithm is characterized by a complexity that increases linearly with the number of users, like the SIC 2 algorithm but unlike the SIC 1 algorithm, whose complexity grows quadratically with N [15]. In evaluating the complexity of the SIC 1 algorithm, we considered the recursive implementation proposed in [15] for the required matrix inversion. Even with this optimization, the matrix inversion represents the bottleneck of the algorithm from a complexity point of view.

Finally, we point out that the values reported in Table 3.1 were computed assuming that the N users all interfere on each other, and that the detector tries to cope with all of them. In general, the value of N in Table 3.1 should be read not as the number of users that actually interfere, but as the number of users that the detector assume to interfere. For example, when the number of users is large, it is mandatory for the complexity of the detector to be reduced that only a few of them are considered (clearly those characterized by the largest interference weights).

We now consider the BER performance. The simulation results reported in Fig. 3.5 refer to the case of $N = 4$ users, all transmitting with the same power. For simplicity, constant cross-correlation of the spreading sequences is also assumed, that is

$$G_{n,m}/G_{n,n} = \gamma \in (0,1), \quad \forall m \neq n \; .$$

All users employ the same non-recursive rate-1/2 convolutional code with gen-

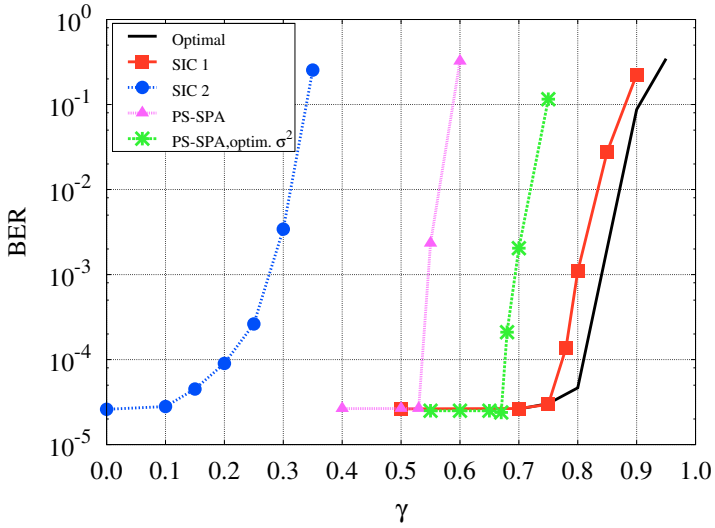

Figure 3.5: CDMA system with $N = 4$ synchronous users and SNR $= 1.35$ dB. All interferers are characterized by the same value of γ.

erators $(23, 35)_8$, a BPSK modulation, and a different random interleaver of length 256 bits. A maximum of 15 iterations between detector and decoder are allowed. We compare the BER performance of the considered algorithms versus γ, at a fixed SNR of 1.35 dB. Aimed at low-latency detection, all algorithms are implemented in their parallel version. The performance of the optimal MAP multiuser detector is also shown for comparison. It should just be considered as a reference benchmark for the performance of the suboptimal algorithms, since its complexity is unaffordable in all practical scenarios [15].

Note that the various algorithms achieve the ISI-free BER (about $2.5 \cdot 10^{-5}$) at different values of γ, which implies that they can manage different levels of interference. Namely, the SIC 1 algorithm is able to completely cancel out the interference for any value of γ up to 0.75, while the SIC 2 algorithm achieves the ISI-free performance only if $\gamma < 0.1$. For the proposed PS-SPA algorithm described in Section 3.3, in Fig. 3.5 we report two curves, with and without the optimization of σ^2, respectively. Interestingly, the same technique was found

not to improve at all the performance of the SIC 1 and SIC 2 algorithms. Note that the PS-SPA with optimized σ^2 achieves the ISI-free performance when $\gamma < 0.68$. In practice, the proposed linear-complexity algorithm significantly outperforms the linear-complexity SIC 2 algorithm, and approaches the performance of the quadratic-complexity SIC 1 algorithm. In scenarios with a large number of users, the proposed algorithm can thus provide the most convenient performance/complexity tradeoff.

3.5.3 Spectrally-efficient FDM systems

Let us finally consider an FDM scenario in which $U = 3$ users, equally spaced in frequency, transmit at the same power by using an 8-PSK modulation with a square-root raised-cosine shaping pulse having roll-off 0.35. We define the normalized channel spacing as $FT = |f^{(i)} - f^{(i-1)}|T$. In these conditions, adjacent users do not interfere when $FT = 1.35$. Each user employs an outer non-recursive rate-1/2 convolutional code with generator polynomials $(23, 35)_8$, concatenated with the Gray mapper through a random bit interleaver (different for each user). At the receiver, the described suboptimal MUDs are employed as SISO detector, and iterative detection/decoding is allowed with a maximum of 10 iterations. As a possible field of application, we consider the reverse link of a satellite system, following the Digital Video Broadcating Return Channel via Satellite (DVB-RCS) standard [73], where a trasponder is shared by multiple users using an FDM access strategy. For this reason, we consider the case of short data bursts—codewords of length 512 bits are adopted.

In Fig. 3.6, we show the BER curve for the middle user when using the proposed PS-SPA, the SIC 1, or the SIC 2 algorithm. Since the interference from adjacent channels dominates, we can reduce the complexity of MUD receivers assuming that the interference among non-adjacent users is negligible. In other words, $\boldsymbol{G}$ is a block tridiagonal matrix where

$$\boldsymbol{G}^{(i,j)} = \mathbf{0} \text{ for } |i - j| \geq 1 \,.$$

To further limit the receiver complexity, we assume that the memory associated

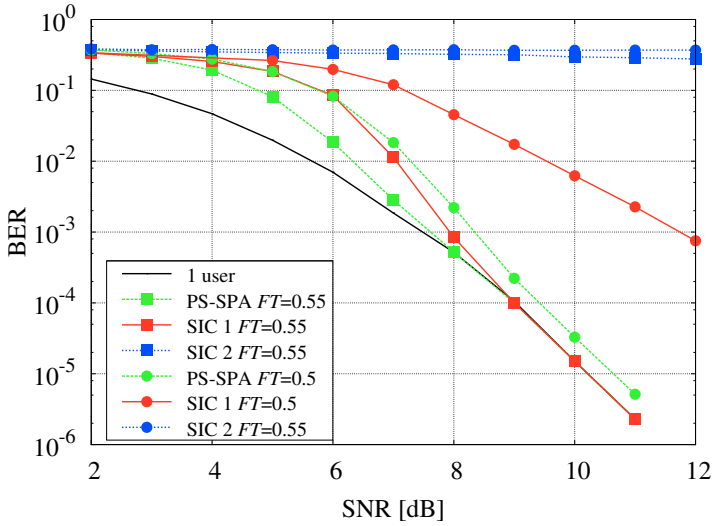

Figure 3.6: FDM systems with $U = 3$ synchronous users. A 8-PSK and a rate 1/2 convolutional code are emplyed.

with the interference is of only three symbols, i.e., $G_{n,m}^{(i,i\pm1)} = 0$ for $|n-m| \geq 1$. We remark that the above approximations are exploited only by the receiver. As mentioned, all algorithms are implemented in the logarithmic domain. As far as the proposed graph-based is concerned, for computing messages $\{\nu_{n,m}\}$ as in (3.16) we also used the approximation $\log(e^{x_1} + e^{x_2}) \approx \max(x_1, x_2)$ [40].

In Fig. 3.6, we consider two channel spacings, resulting in strong-interference scenarios, and in both cases the proposed algorithm achieves the best performance among the considered suboptimal receivers. For $FT = 0.55$, the PS-SPA and the SIC 1 algorithm exhibit a good performance despite the presence of strong interference, achieving the interference-free performance for SNR = 8 dB and for SNR = 9 dB, respectively. When the spacing is $FT = 0.5$, the performance gain of the PS-SPA increases. In particular, at a BER of 10^{-3} the proposed algorithm exhibits a gain of about 3.5 dB with respect to the SIC 1 algorithm, despite the lower computational complexity. Moreover, the loss of the proposed algorithm with respect to the interference-free case is only about

Table 3.2: FDM systems: Computational load per symbol, per iteration for the middle user in the scenario considered in Fig. 3.6.

Algorithm	Additions	LUT accesses
Proposed	872	0
SIC 1	2150	2140
SIC 2	77	115

0.8 dB. In both scenarios, the SIC 2 algorithm is definitely unable to manage the interference.

In Table 3.2, we show the computational complexity of the considered MUD algorithms in the same scenario of Fig. 3.6. We report the number of additions between two real arguments and accesses to LUT per symbol and per iteration for the middle user in case of a logarithmic-domain implementation. The operations performed only at the first iteration have been neglected. This table clearly shows that the proposed algorithm has a complexity much lower than that of SIC 1 algorithms.

3.6 Conclusions

We presented novel algorithms for SISO detection over linear channels impaired by AWGN. These algorithms, which have been derived by applying the SPA to a suitably-designed FG, are characterized by a complexity that grows only linearly with the number of interferers.

Focussing on some selected scenarios, we have shown that the proposed receivers represent the best trade-off between performance and complexity, approaching or even outperforming the performance provided by much more complex receivers.

Chapter 4

Conclusions

In this thesis we considered the application of reduced-complexity MUD techinques to spectrally-efficient wireless communication systems.

In Chapter 2, we focused on satellite FDM-CPM systems where channels are allowed to overlap in frequency to increase the SE. We extended to this scenario some well known SIC algorithms proposed for CDMA systems, which are derived relying on a Gaussian approximation of the MAI. We also introduced a novel detection scheme using the framework based on FGs and the SPA. The new proposed detection algorithm is the most effective one in terms of performance and computational complexity among the considered suboptimal receivers. Furthermore, we investigated the ultimate performance limits of FDM-CPM systems, computing the IR and the SE. In particular, we optimized the channel spacing using simple binary and quaternary RC and REC CPMs to maximize the SE. This analysis revealed that it is more convenient to consider frequency spacings between the channels much lower than those usually employed in state-of-the-art systems to limit the interference from adjacent users, thus providing a better tradeoff between degradation of the IR due to the interference and usage of the available spectrum. Moreover, it was shown that for low SEs, REC and RC formats perform similarly. However, REC allows achieving higher SEs.

We also considered practical SCCPM schemes using the suboptimal graph-based multiuser receiver, showing that theoretical limits predicted by the information rate analysis can be approached.

Finally, we considered more realistic scenarios of channels affected by time-varying PN and carrier phase and frequency uncertainty. We extended the graph-based detection algorithm for MUD in the presence of PN and proposed new DA multiuser phase and frequency synchronization schemes. The simulation results showed that the proposed schemes allow to implement transmission schemes with an unprecedented SE at a price of a limited complexity increase with respect to a classical single-user receiver which neglects the interference.

In Chapter 3, we considered linear channels impaired by AWGN. For this general model, which describes a large variety of scenarios, novel algorithms for SISO detection were proposed. These new schemes were derived by applying the SPA to a suitably-designed FG and are characterized by a complexity which grows only linearly with the number of interferers. We evaluated the effectiveness of the proposed solutions in some selected scenarios, such as CDMA and FDM systems with MAI, comparing them with more classical interference cancellation algorithms. We showed that the proposed receivers represent the best trade-off between performance and complexity, approaching or even outperforming the performance provided by much more complex receivers.

List of Pubblications

Journal papers

- A. Barbieri, A. Piemontese, and G. Colavolpe, *On the ARMA approximation for fading channels described by the Clarke model with applications to Kalman-based receivers*, IEEE Trans. Wireless Commun., vol. 8, pp. 535-540, February 2009.

- A. Piemontese and G. Colavolpe, *A Novel Graph-Based Suboptimal Multiuser Detector for FDM-CPM Transmissions*, IEEE Trans. Wireless Commun., vol. 9, pp. 2812-2819, September 2010.

- G. Colavolpe, D. Fertonani, and A. Piemontese, *Graph-Based Detection over Linear Channels Using the Ungerboeck Observation Model*, submitted to IEEE Journal of Selected Topics in Signal Processing, Special issue on Soft Detection for Wireless Transmission.

- A. Piemontese, N. Mazzali, and G. Colavolpe, *Improving the spectral efficiency of FDM-CPM systems through packing and multiuser processing*, submitted to International Journal of Satellite Communications and Networking. **Invited paper**.

Conference papers

- A. Barbieri, A. Piemontese, and G. Colavolpe, *On the ARMA approximation for frequency-flat Rayleigh fading channels*, in Proc. IEEE Intern.

Symp. Inform. Theory (ISIT'07), Nice, France, June 2007, pp. 1211-1215.

- A. Barbieri, A. Cero, A. Piemontese, and G. Colavolpe, *Markov capacity of continuous phase modulations*, in Proc. IEEE Intern. Symp. Inform. Theory (ISIT'07), Nice, France, June 2007, pp. 161-165.

- A. Barbieri, G. Colavolpe, D. Fertonani, and A. Piemontese, *Novel graph-based algorithms for interference cancellation in CDMA systems*, in Proc. IEEE International Workshop on Signal Processing Advances for Wireless Communications (SPAWC'09), Perugia, Italy, June 2009, pp. 712-716.

- A. Piemontese and G. Colavolpe, *A novel graph-based soft interference cancellation algorithm for FDM-CPM satellite systems*, in Proc. IEEE Intern. Symp. on Inform. Theory (ISIT'09), Seoul, Korea, June 2009, pp. 2271-2275.

- A. Piemontese, N. Mazzali, and G. Colavolpe, *Improving the spectral efficiency of FDM-CPM systems through packing and multiuser processing*, in Proc. 5th Advanced Satellite Mobile Systems Conference and 11th International Workshop on Signal Processing for Space Communications (ASMS&SPSC 2010), Cagliari, Italy, September 2010, pp. 106-113. **Best paper award**.

- A. Piemontese, A. Graell i Amat and G. Colavolpe, *Information-theoretic analysis and practical coding schemes for spectrally efficient FDM-CPM systems*, in Proc. 6th Intern. Symp. on Turbo Codes & Iterative Information Processing, Brest, France, September 2010, pp. 275-279.

Patents

- G. Colavolpe and A. Piemontese, *Reduced complexity FDM-CPM dectector with multiple access interference cancellation*, assigned to Newtec Cy, Belgium, International patent application n. PCT/EP2010/059144, June 2010.

Technical reports

- A. Barbieri and A. Cero and G. Colavolpe and D. Fertonani and A. Piemontese, *BSDT – Technical Note TN05: Reduced-complexity CPM detector*, June 2007, ESA Contract No. 19370

- A. Barbieri and A. Cero and G. Colavolpe and D. Fertonani and A. Piemontese, *BSDT – Technical Note TN14: Shaper-Precoder Optimization from a Capacity Point of View for CPM Signals*, June 2007, ESA Contract No. 19370

- A. Barbieri and A. Cero and G. Colavolpe and D. Fertonani and A. Piemontese, *BSDT – Technical Note TN20: CPM schemes for high spectral efficiencies*, January 2009, ESA Contract No. 19370

Bibliography

[1] B. F. Beidas, H. El Gamal, and S. Kay, "Iterative interference cancellation for high spectral efficiency satellite communications," *IEEE Trans. Commun.*, vol. 50, no. 1, pp. 31–36, Jan. 2002.

[2] G. Gallinaro and R. Rinaldo, "Assessment of potentiality of adjacent channel interference mitigation in a low-rate TDMA system," in *Proc. Intern. Work. on Signal Processing for Space Commun.*, Rhodes Island, Greece, October 2008.

[3] S. Verdú, *Multiuser Detection*, Cambridge University Press, Cambridge, UK, 1998.

[4] F. R. Kschischang, B. J. Frey, and H.-A. Loeliger, "Factor graphs and the sum-product algorithm," *IEEE Trans. Inform. Theory*, vol. 47, pp. 498–519, Feb. 2001.

[5] G. Colavolpe, A. Barbieri, and G. Caire, "Algorithms for iterative decoding in the presence of strong phase noise," *IEEE J. Select. Areas Commun.*, vol. 23, no. 9, pp. 1748–1757, Sept. 2005.

[6] G. Colavolpe and G. Germi, "On the application of factor graphs and the sum-product algorithm to ISI channels," *IEEE Trans. Commun.*, vol. 53, pp. 818–825, May 2005.

[7] G. Colavolpe, "On LDPC codes over channels with memory," *IEEE Trans. Wireless Commun.*, vol. 5, no. 7, pp. 1757–1766, July 2006.

[8] A. Barbieri and G. Colavolpe, "Soft-output decoding of rotationally invariant codes over channels with phase noise," *IEEE Trans. Commun.*, vol. 55, no. 11, pp. 2125–2133, Nov. 2007.

[9] A. Barbieri and G. Colavolpe, "Simplified soft-output detection of CPM signals over coherent and phase noise channels," *IEEE Trans. Wireless Commun.*, vol. 6, no. 7, pp. 2486–2496, July 2007.

[10] G. Colavolpe and A. Barbieri, "On MAP symbol detection for ISI channels using the Ungerboeck observation model," *IEEE Commun. Letters*, vol. 9, no. 8, pp. 720–722, Aug. 2005.

[11] K. R. Narayanan and G. L. Stüber, "Performance of trellis-coded CPM with iterative demodulation and decoding," *IEEE Trans. Commun.*, vol. 49, pp. 676–687, Apr. 2001.

[12] P. Moqvist and T. M. Aulin, "Serially concatenated continuous phase modulation with iterative decoding," *IEEE Trans. Commun.*, vol. 49, pp. 1901–1915, Nov. 2001.

[13] A. Graell i Amat, C. A. Nour, and C. Douillard, "Serially concatenated continuous phase modulation for satellite communications," *IEEE Trans. Wireless Commun.*, vol. 8, pp. 3260–3269, June 2009.

[14] P. Moqvist, *Multiuser serially concatenated continuous phase modulation*, Ph.D. thesis, Chalmers University of Technology, Goteborg, Sweden, 2002.

[15] X. Wang and H. V. Poor, "Iterative (turbo) soft interference cancellation and decoding for coded CDMA," *IEEE Trans. Commun.*, vol. 47, pp. 1046–1061, July 1999.

[16] H. El Gamal and E. Geraniotis, "Iterative multiuser detection for coded CDMA signals in AWGN and fading channels," *IEEE J. Select. Areas Commun.*, vol. 18, pp. 30–41, Jan. 2000.

[17] J. Boutros and G. Caire, "Iterative multiuser joint decoding: unified framework and asymptotic analysis," *IEEE Trans. Inform. Theory*, vol. 48, no. 7, pp. 1772–1793, July 2002.

[18] A. Barbieri, D. Fertonani, and G. Colavolpe, "Time-frequency packing for linear modulations: spectral efficiency and practical detection schemes," *IEEE Trans. Commun.*, vol. 57, pp. 2951–2959, Oct. 2009.

[19] V. Sharma and S. K. Singh, "Entropy and channel capacity in the regenerative setup with application to Markov channels," in *Proc. IEEE International Symposium on Information Theory*, Washington, DC, June 2001, p. 283.

[20] H. D. Pfister, J. B. Soriaga, and P. H. Siegel, "On the achievable information rates of finite-state ISI channels," in *Proc. IEEE Global Telecommun. Conf.*, San Antonio, TX, 2001, pp. 2992–2996.

[21] D. M. Arnold, H.-A. Loeliger, P. O. Vontobel, A. Kavčič, and W. Zeng, "Simulation-based computation of information rates for channels with memory," *IEEE Trans. Inform. Theory*, vol. 52, no. 8, pp. 3498–3508, Aug. 2006.

[22] T. M. Cover and J. A. Thomas, *Elements of Information Theory*, John Wiley & Sons, Inc., New York, 1991.

[23] L. R. Bahl, J. Cocke, F. Jelinek, and J. Raviv, "Optimal decoding of linear codes for minimizing symbol error rate," *IEEE Trans. Inform. Theory*, vol. 20, pp. 284–287, Mar. 1974.

[24] J. B. Anderson, T. Aulin, and C.-E. W. Sundberg, *Digital Phase Modulation*, Plenum Press, New York, 1986.

[25] B. E. Rimoldi, "A decomposition approach to CPM," *IEEE Trans. Inform. Theory*, vol. 34, pp. 260–270, Mar. 1988.

[26] H. Meyr, M. Oerder, and A. Polydoros, "On sampling rate, analog prefiltering, and sufficient statistics for digital receivers," *IEEE Trans. Commun.*, vol. 42, pp. 3208–3214, Dec. 1994.

[27] A. A. M. Saleh, "Frequency-independent and frequency-dependent nonlinear models of TWT amplifiers," *IEEE Trans. Commun.*, vol. 29, pp. 1715–1720, Nov. 1981.

[28] ETSI TR 102 376 V1.1.1 (2005-02), Digital Video Broadcasting (DVB) - User Guidelines for the second generation system for Broadcasting, Interactive Services, News Gathering and other broadband satellite applications (DVB-S2), 2005.

[29] R. De Gaudenzi, A. Guillén i Fàbregas, and Martinez A., "Performance analysis of turbo-coded APSK modulations over nonlinear satellite channels," *IEEE Trans. Wireless Commun.*, vol. 5, pp. 2396–2407, Sept. 2006.

[30] A. Vannucci and R. Raheli, "Optimal sequence detection based on oversampling for bandlimited nonlinear channels," in *Proc. IEEE Intern. Conf. Commun.*, Atlanta, U.S.A., 1995, pp. 417–421.

[31] J. E. Mazo, "Faster-than-Nyquist signaling," *Bell System Tech. J.*, vol. 54, pp. 1450–1462, Oct. 1975.

[32] J. E. Mazo and H. J. Landau, "On the minimum distance problem for faster-than-Nyquist signaling," *IEEE Trans. Inform. Theory*, pp. 1420–1427, Nov. 1988.

[33] A. Liveris and C. N. Georghiades, "Exploiting faster-than-Nyquist signaling," *IEEE Trans. Commun.*, pp. 1502–1511, Sept. 2003.

[34] F. Rusek and J. B. Anderson, "On information rates of faster than Nyquist signaling," in *Proc. IEEE Global Telecommun. Conf.*, San Francisco, CA, U.S.A., Nov. 2006.

[35] F. Rusek and J. B. Anderson, "Maximal capacity partial response signaling," in *Proc. IEEE Intern. Conf. Commun.*, June 2007, pp. 821–826.

[36] A. R Calderbank and L. H. Ozarow, "Nonequiprobable signalling on the Gaussian channel," *IEEE Trans. Inform. Theory*, vol. 36, pp. 726–740, July 1990.

[37] A. Barbieri, D. Fertonani, and G. Colavolpe, "Spectrally-efficient continuous phase modulations," *IEEE Trans. Wireless Commun.*, vol. 8, pp. 1564–1572, Mar. 2009.

[38] U. Mengali and M. Morelli, "Decomposition of M-ary CPM signals into PAM waveforms," *IEEE Trans. Inform. Theory*, vol. 41, pp. 1265–1275, Sept. 1995.

[39] G. Colavolpe and R. Raheli, "Noncoherent sequence detection of continuous phase modulations," *IEEE Trans. Commun.*, vol. 47, pp. 1303–1307, Sept. 1999.

[40] P. Roberston, E. Villebrun, and P. Hoeher, "Optimal and sub-optimal maximum a posteriori algorithms suitable for turbo decoding," *European Trans. Telecommun.*, vol. 8, no. 2, pp. 119–125, March/April 1997.

[41] N. Merhav, G. Kaplan, A. Lapidoth, and S. Shamai Shitz, "On information rates for mismatched decoders," *IEEE Trans. Inform. Theory*, vol. 40, no. 6, pp. 1953–1967, Nov. 1994.

[42] S. ten Brink, "Convergence behavior of iteratively decoded parallel concatenated codes," *IEEE Trans. Commun.*, vol. 49, no. 10, pp. 1727–1737, Oct. 2001.

[43] F. Brännström, L. K. Rasmussen, and A. J. Grant, "Convergence analysis and optimal scheduling for multiple concatenated codes," *IEEE Trans. Inform. Theory*, vol. 51, no. 9, pp. 3354–3364, Sept. 2005.

[44] G. Colavolpe, G. Ferrari, and R. Raheli, "Extrinsic information in iterative decoding: a unified view," *IEEE Trans. Commun.*, vol. 49, pp. 2088–2094, Dec. 2001.

[45] U. Mengali and M. Morelli, "Data-aided frequency estimation for burst digital transmission," *IEEE Trans. Commun.*, vol. 45, pp. 23–25, Jan. 1997.

[46] A. Barbieri and G. Colavolpe, "On the Cramer-Rao bound for carrier frequency estimation in the presence of phase noise," *IEEE Trans. Wireless Commun.*, vol. 6, pp. 575–582, Feb. 2007.

[47] J. G. Proakis, *Digital Communications*, McGraw-Hill, New York, 4th edition, 2001.

[48] G. D. Forney, Jr., "Maximum-likelihood sequence estimation of digital sequences in the presence of intersymbol interference," *IEEE Trans. Inform. Theory*, vol. 18, pp. 284–287, May 1972.

[49] J. A. C. Bingham, "Multicarrier modulation for data transmission: An idea whose time has come," *IEEE Commun. Mag.*, pp. 5–14, May 1990.

[50] Ying Zhu, Taikun Cheng, Krishnamoorthy Sivakumar, and Benjamin J. Belzer, "Markov random field detection on two-dimensional intersymbol interference channels," *IEEE Trans. Signal Processing*, pp. 2639–2648, July 2008.

[51] Yunxiang Wu, Joseph A. O'Sullivan, Naveen Singla, and Ronald S. Indeck, "Iterative detection and decoding for separable two-dimensional intersymbol interference," *IEEE Trans. on Magnetics*, pp. 2115–2120, July 2003.

[52] V. Tarokh, N. Seshadri, and A. R. Calderbank, "Space-time codes for high data rate wireless communication: Performance criterion and code construction," *IEEE Trans. Inform. Theory*, vol. 44, no. 2, pp. 744–765, Mar. 1998.

[53] J. Hu and T. M. Duman, "Graph-based detection algorithms for layered space-time architectures," *IEEE J. Select. Areas Commun.*, vol. 26, pp. 269–280, Feb. 2008.

[54] M. Tüchler, A. C. Singer, and R. Koetter, "Minimum mean square error equalization using *a priori* information," *IEEE Trans. Signal Processing*, vol. 50, pp. 673–683, Mar. 2002.

[55] M. Tüchler, R. Koetter, and A. C. Singer, "Turbo equalization: Principles and new results," *IEEE Trans. Commun.*, vol. 50, pp. 754–767, May 2002.

[56] C. Douillard, M Jezequel, C. Berrou, A. Picart, P. Didier, and A. Glavieux, "Iterative correction of intersymbol interference: turbo-equalization," *European Trans. Telecommun.*, vol. 6, no. 5, pp. 507–511, September/October 1995.

[57] G. D. Forney, Jr., "Lower bounds on error probability in the presence of large intersymbol interference," *IEEE Trans. Commun.*, vol. 20, pp. 76–77, Feb. 1972.

[58] G. Ungerboeck, "Adaptive maximum likelihood receiver for carrier-modulated data-transmission systems," *IEEE Trans. Commun.*, vol. com-22, pp. 624–636, May 1974.

[59] T. Richardson and R. Urbanke, "The capacity of low density parity check codes under message passing decoding," *IEEE Trans. Inform. Theory*, vol. 47, pp. 599–618, Feb. 2001.

[60] G. Colavolpe, "Design and performance of turbo Gallager codes," *IEEE Trans. Commun.*, vol. 52, pp. 1901–1908, Nov. 2004.

[61] J. Zhang and M. P. C. Fossorier, "Shuffled iterative decoding," *IEEE Trans. Commun.*, vol. 2, no. 53, pp. 209–213, Feb. 2005.

[62] D. Fertonani, A. Barbieri, and G. Colavolpe, "Reduced-complexity BCJR algorithm for turbo equalization," *IEEE Trans. Commun.*, vol. 55, no. 12, pp. 2279–2287, Dec. 2007.

[63] Q. Guo and L. Ping, "LMMSE turbo equalization based on factor graph," *IEEE J. Select. Areas Commun.*, vol. 26, pp. 311–319, Feb. 2008.

[64] F. Rusek, M. Loncar, and A. Prlja, "A comparison of Ungerboeck and Forney models for reduced-complexity ISI equalization," in *Proc. IEEE Global Telecommun. Conf.*, Washington, DC, U.S.A., Nov. 2007.

[65] A. Hafeez and W. E. Stark, "Decision feedback sequence estimation for unwhitened ISI channels with applications to multiuser detection," *IEEE J. Select. Areas Commun.*, vol. 16, no. 9, pp. 1785–1795, Dec. 1998.

[66] D. Yachil, J. Davidson, and B. Bobrosky, "Low complexity multi-channel synchronization for satellite systems with adjacent channel interference," *International Journal of Satellite Communications and Networking*, vol. 24, pp. 1–22, 2006.

[67] J. Grotz, B. Ottersten, and J. Krause, "Joint channel synchronization under interference limited conditions," *IEEE Trans. Wireless Commun.*, vol. 6, no. 10, pp. 3781–3789, Oct. 2007.

[68] L. Rugini, P. Banelli, and G. Leus, "Simple equalization of time-varying channels for OFDM," *IEEE Communications Letters*, pp. 619–621, July 2005.

[69] Kai Tu, Dario Fertonani, Tolga M. Duman, Milica Stojanovic, John G. Proakis, and Paul Hursky, "Mitigation of intercarrier interference for OFDM over time-varying underwater acoustic channels," *IEEE Journal of Oceanic Engineering*, to appear in 2011.

[70] S. ten Brink, G. Kramer, and A. Ashikhmin, "Design of low-density parity-check codes for modulation and detection," *IEEE Trans. Commun.*, vol. 52, pp. 670–678, Apr. 2004.

[71] D. Fertonani, A. Barbieri, and G. Colavolpe, "Novel graph-based algorithms for soft-output detection over dispersive channels," in *Proc. IEEE Global Telecommun. Conf.*, New Orleans, LA, USA, Nov.-Dec. 2008.

[72] P. Robertson, E. Villebrun, and P. Hoeher, "A comparison of optimal and suboptimal MAP decoding algorithms operating in the log domain," in *Proc. IEEE Intern. Conf. Commun.*, Seattle, WA, 1995, pp. 1009–1013.

[73] ETSI, "EN 301 790: DVB-RCS V1.4.1, Digital Video Broadcasting (DVB); Interaction Channel for Satellite Distribution Systems," 2003.

Acknowledgements

First and foremost, I wish to express my most sincere gratitude to my advisor Prof. Giulio Colavolpe. I would like to thank him for his continuous and essential guidance, for all the inspiring discussions we had, and for the help with scientific and non-scientific problems.

I would like to thank my advisor Prof. Alexandre Graell i Amat, for his help with this research, for his comments on this thesis, and for introducing me to the French Departement.

I thank Newtec Cy for supporting this research. In particular, I would like to thank Dr. Daniel Delaruelle and Dr. Alain Rolle for all the fruitful and stimulating discussions on FDM-CPM topic. My thanks also go to Turbo Concept, in particular to Dr. Pierre Wadier for the help with scientific and technical problems.

I thank my former and present colleagues at the Information Engineering Department of the University of Parma.

I am grateful to the Electronic Departement of Télécom Bretagne, in particular to Prof. Catherine Douillard for her support and for the welcome in Brest.

Finally, a special thank to Giovanni and to my family, for their infinite love and support. I dedicate this thesis to you.